LIMITING FACTORS IN ACOUSTIC DENSITY SEPARATION OF CARBON PARTICLES IN AIR

Prepared for

Professor Jonathan Tapson

The University of Cape Town

Prepared by

David Karpul

KRPDAV002

Submitted to the Department of Electrical Engineering, University of Cape Town, in fulfilment of the requirements for the degree: Masters of Science in Electrical Engineering.

17 November 2009

Key Words: **Acoustic Density Separation, Smoke Stacks, Acoustic Force Field, Particle Filtration, Global Warming, Pollution**

DECLARATION

I declare that the work contained in this thesis is my own and no part was created by another party. All references and sources have been appropriately acknowledged.

This work is submitted to the Department of Electrical Engineering, University of Cape Town, in fulfilment of the requirements for the degree: Masters of Science in Electrical Engineering, and has not been submitted for any other academic purposes before this.

David Karpul
University of Cape Town
Rondebosch
Cape Town
17 November 2009

ABSTRACT

Particles suspended in a fluid that is exposed to an acoustic standing wave experience a time-averaged force that drives them to either the pressure nodes or anti-nodes of the wave. Several filter designs have been successfully implemented using this force to filter small particles in liquids with low flow rates and small cross-sectional areas. It has been suggested that the filtration of small solid particles out of a gas, such as carbon in air (smoke), would be a possible application of acoustic density separation.

The emissions created by the combustion of hydrocarbons used in industrial processes, electricity production and transport significantly damage human health and the world at large. Particulate matter released, primarily by power plants, is currently removed from the emissions by highly space consuming and expensive equipment. The creation of a new type of particulate filter, which is both more cost effective and less space consuming, would be beneficial to the industry and consequently the environment at large.

This study shows the limiting factors, in both power requirements and design factors, of an acoustic filter designed for filtering smoke particles across large cross-sectional areas at high flow rates, as in the case of an industrial smoke stack. It is shown that while filtration is possible, the power needed is impractical. It is also shown that operating the filter above a particular threshold intensity the energy usage of the filter is optimised.

ACKNOWLEDGMENTS

The author David Karpul wishes to acknowledge the important role of the University of Cape Town, its facilities and technical staff, without whom this research would not be possible. In particular, the author thanks the Sensors and Actuators Group, the Acoustics Group, Steven Schrire and Samuel Ginsberg.

The author further wishes to acknowledge his family and friends, many of whom have not only lent their support, but their time to aid with editing. Specifically the author wishes to acknowledge, Gregory Cohen, his father Mendel, Stuart Lightbody and Stanley Walton for their editing efforts.

Special acknowledgment goes to the following people:

Cesarina Edmonds-Smith – for providing use of several pieces of apparatus from the chemistry department of UCT;

Michael Rapson – for providing a fresh perspective whenever needed, and aiding with technical knowledge wherever he could; and,

Jonathan Tapson – for being an ever understanding and patient supervisor. For the sake of engineers to be, may the well of your patience never run dry.

TABLE OF CONTENTS

LIST OF FIGURES

LIST OF TABLES

1 INTRODUCTION

In spite of the prediction made by Charles H. Duell, the Commissioner of the U.S. Office of Patents in 1899 that: “Everything that can be invented has been invented”, novel invention and technological development have been the cornerstone of the twentieth and twenty first centuries. While further development often creates more problems than it solves, humanity’s lust for mastery of all that is within its grasp is insatiable.

In the venture for discovery, failure is never the goal; however, a scientifically proven failure can often have tremendous value since it can not only prevent others from wasting their time searching for that which cannot be found, but can also show that current thinking on the topic is incorrect. For example, consider the null result created in 1887 by Albert Michelson and Edward Morley, which earned Michelson the Nobel Prize. The two scientists set out through years of precise measurements, to measure the *luminiferous aether* wind through which light and electromagnetic waves must travel in the vacuum of space. Their results showed no affect by the *luminiferous aether* wind on the speed of light. Their null result thus inadvertently proved that the speed of light is constant, a fact later confirmed by Albert Einstein’s General Theory of Relativity, and that the *luminiferous aether* as an idea is better left for science fiction novels.

Investigating the crossover of a discovery from its original field of interest into an unrelated field has resulted in many great discoveries, for example the development of statistical methods for analysis of baseball has resulted in the advancement of economics. This thesis seeks to investigate such a crossover. The acoustic force, originally used to demonstrate properties of waves, and now also used to aid in the filtering of small cells from water, has been thought to have applications in removing particulate matter from the smoke created in industrial processes.

The following chapters highlight the need to address the problem of pollution, and specifically the need to reduce the emission of damaging substances into the environment. They further present a design to address the problem through the application of acoustic force fields to create a new type of air filter, and show that such a design is infeasible.

1.1 GOAL AND SCOPE

The goal of this research is to investigate the application of acoustic filtering in industrial smoke stacks as a means of reducing the amount of pollution released into the environment.

The research covers a comprehensive background to the topics both relating to the technology required to implement acoustic filtering in smokes stacks, and the environmental issues that the solution attempts to address.

This thesis will also cover the modelling of a realistic application scenario and show in theory the effectiveness of the proposed design. It will show practical experiments that attempt to demonstrate the conversion from theory to practical, and the experimental measurement of various required parameters.

This thesis does not present a comprehensive study into the physics, operation or design of smoke stacks, their exhaust fumes or their direct effect on the environment but rather only covers that which is essential to know in order to answer the basic question asked by the research – *is it possible?*

Though the theory behind general acoustic waves and how to model them is covered, a study into the nature of the resonance of complex structures is not, as it would unnecessarily increase the scope of the research.

1.2 DEVELOPMENT

The diagram below illustrates the conceptual flow of this thesis: starting with background chapters; moving onto the design and implementation of a rig to test the theory of operation of an acoustic filter; the theory governing the results found in practical work is investigated; and, finally conclusions are drawn. A block in the diagram does not necessarily correlate directly to a chapter of the thesis. The arrows show the interconnection of the concepts and allow the reader to see which areas of the thesis are dependent on previous sections and which can be independently read.

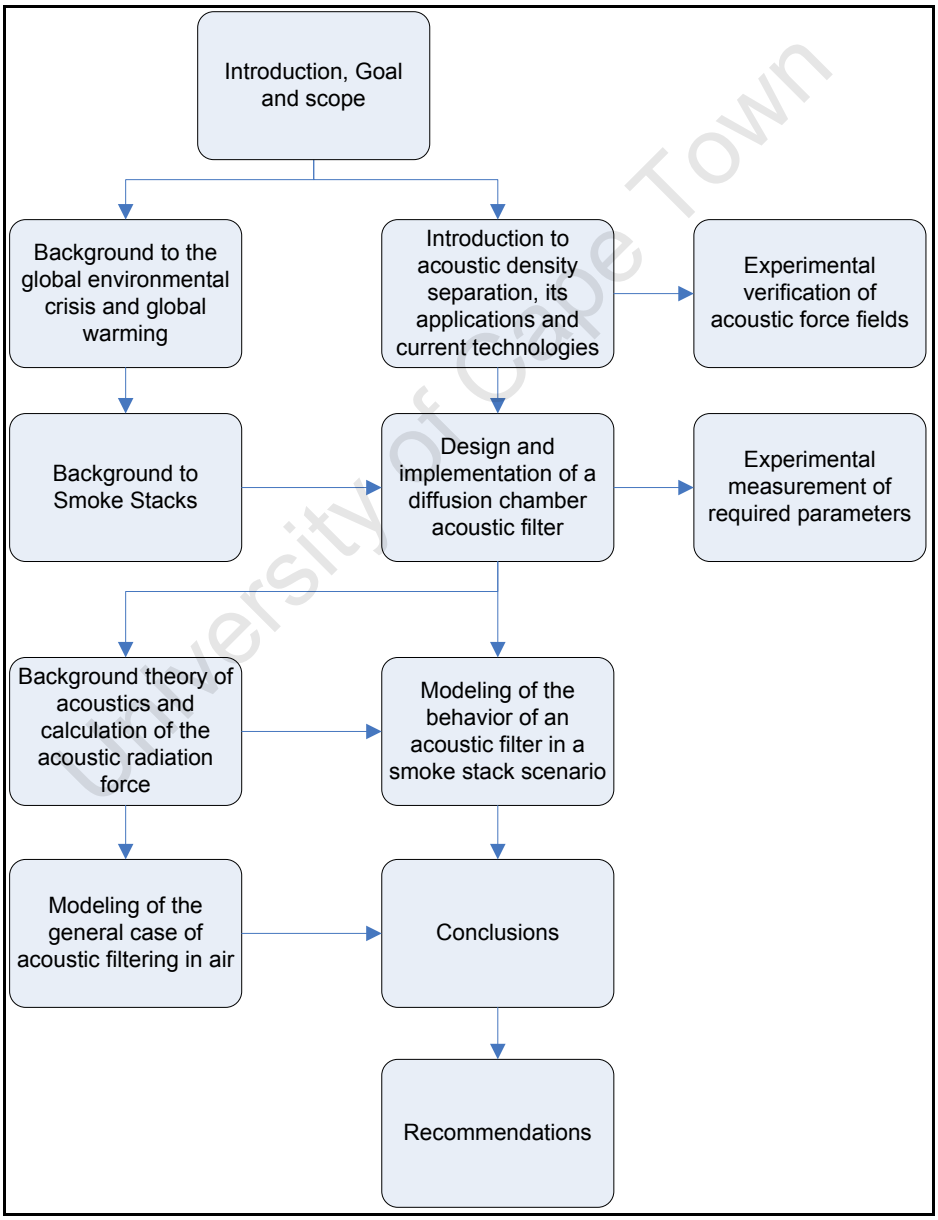

Figure 1 Development diagram showing the interconnection of topics in this thesis.

2 GLOBAL ENVIRONMENTAL CRISIS

This thesis primarily deals with the design and modelling of an acoustic air filter, but it is important to keep in mind the reason why such a technology would be useful. Modern science has shown that the Earth has entered a stage of global environmental crisis. Projections show that in the short term, continued emissions of pollutants into the atmosphere will be severely damaging to human and animal health, while in the long term global warming may cause a runaway effect that could eliminate our species. Other environmental issues such as deforestation and the extinction of species are ultimately all interconnected, but will not be dealt with here.

2.1 PRIMARY AIR POLLUTANTS

Historically air pollution has been dealt with by considering its direct effect on human life. In 1952 four thousand excess deaths in London were attributed to a week of particularly bad smog in the city. In 1955 the United States congress passed the Air Pollution Control Act which focused on the *six criteria air pollutants* primarily created through combustion processes. The act would serve as the basis of air pollution control for the next forty to fifty years in the US [**1**].

The burning of hydro-carbons is the main source of air pollution and is essential to many forms of electricity production, industrial furnaces and other chemical processes requiring large amounts of heat. We can represent the ideal burning of a pure hydro-carbon such as methane (CH_4) as [**1**]:

$$CH_4 + 2O_2 \rightarrow CO_2 + 2H_2O, \tag{1}$$

where: O_2 is a molecule of oxygen; CO_2 is a molecule of carbon dioxide; and, H_2O is water.

In practice, many factors affect the by-products of a combustion process. Factors such as: insufficient heat; lack of enough oxygen; and insufficient reaction time, cause the fuel to not fully oxidize. In this case some of the carbon from the fuel will be released as carbon monoxide (CO) and some of the unburned fuel will remain as partially combusted hydro-carbons and be released as particulate matter. In practice, air is used instead of pure oxygen. Air contains only 21 percent oxygen and is mostly nitrogen (N_2) (78 percent). In sufficiently high temperatures the nitrogen also reacts with the oxygen, producing various nitrogen oxides (NO_x). Most fuels also have a variety of impurities including: nitrogen, sulphur (S), lead (Pb) and incombustible materials known as ash.

These impurities produce additional NO_x, sulfur oxides (SO_x), lead, particulate matter and ash. The resulting reaction can be represented as:

$$Fuel(H, C, S, N, Pb, ash) + air(N_2 + O_2) \rightarrow emissions(CO_2, H_2O, CO, NO_x, SO_x Pb, particulates) + ash. \quad (2)$$

This reaction shows five of the *six criteria air pollutants* namely, carbon monoxide, lead, nitrogen dioxide, sulphur dioxide, and particulate matter. The sixth pollutant is a secondary pollutant (not directly created by the combustion process) created from the unburned hydrocarbons that readily vaporize (volatile organic compounds – VOCs) and the nitrogen oxides formed from the reaction above. Together in the presence of sunlight, the VOCs and nitrogen oxides form ground ozone (O_3). These six criteria pollutants have been shown to be of the most concern to human health directly and have been the focus of control legislation over the last fifty years [**1**].

In recent times, the focus on climate change has shown that the greenhouse effect of carbon dioxide (responsible for ±60% of the greenhouse effect [**1**]) and other greenhouse gasses are of major concern, not directly on human health, but rather that they adversely affect the maintenance of an inhabitable environment on this planet. The greenhouse effect and climate change are discussed in a later section, but it suffices to say at this stage that greenhouse gasses have been added to the list of pollutants controlled by various legislations.

2.2 PARTICULATE MATTER

The combustion process extensively used in the production of electricity, industrial processing and in transportation, produces a variety of harmful pollutants including particulate matter. 78% of particulate matter is created by stationary sources in the burning of fuels and industrial processing. Particulate matter is defined as any dispersed matter, solid or liquid. Particles take many forms, and can be approximated by an aerodynamically equivalent sphere with diameters ranging from 0.005 µm to 100 µm [**1**]. This thesis deals with the design of an air filter capable of filtering particulate matter and thus this is the only pollutant considered here.

In a study done of the world's twenty largest cities, all with a population greater than 10 million, by the World Health Organization (WHO) and the United Nations Environment Programme (UNEP) in 1992, on the severity of air contamination by the six criteria pollutants, only particulate matter

repetitively was shown to rank as a serious problem where the WHO guidelines had been exceeded by more than a factor of two.

It is important to note that particles smaller than 0.1 µm tend to coagulate due to Brownian motion and grow to sizes larger than 0.1 µm. Particles larger than 10µm settle relatively quickly having a terminal velocity of 20 cm/min. Thus, study of particles between 0.1 µm and 10 µm is of significant importance [**1**].

2.2.1 Direct Effect of Particulate Matter on Human Health

Particulate matter in the air affects the human respiratory system. The probability of a particle lodging itself in the lungs is related directly to its size. In short, particles larger than 10 µm are removed by the upper respiratory system either by being captured by the nose hairs and coughed or sneezed out, or by being trapped in the tracheobronchial system by mucus, moved to the back of the throat by hair like cilia, and swallowed or spat out. Very fine particles, smaller than 0.5 µm, can enter the lungs and be swept out again in exhalation. Particles between 2 µm and 4 µm are the most likely to form sediment in the lungs.

Particulate matter in the lungs aggravates existing respiratory and cardiovascular diseases, damages lung tissue and has been found to be carcinogenic. Furthermore, organic compounds can attach themselves to the long carbons chains that particulate matter is made out of and enter the lungs causing serious health problems including lung cancer [**1**].

2.2.2 Reducing Particulate Emissions

Reducing the emission of harmful substances has become a priority of modern industrial processes and power plants. Since the 1960's the percentage spent on pollution controls of the total cost of building a new coal power plant has risen from less than five percent to the present day where it stands at over forty percent [**1**]. There are three main forms of controlling the emissions created through a combustion process namely: pre-combustion controls; combustion controls; and, post-combustion controls.

Pre-combustion controls include practices such as selecting fuel that results in less emission of pollutants or treating the fuel to the same end. Combustion controls address factors in the combustion process directly. Combustion controls include practices such as tight temperature

control to reduce emissions created through over heating or under heating in the combustion process. Post-combustion controls attempt to capture and possibly treat emissions such that they are not released into the atmosphere, or are released in a harmless form. The last is the most effective way to treat the release of particulate matter and as a result, several technologies have been designed to remove particulate matter from the exhaust gasses of a combustion process.

There are three main forms of particulate control. Centrifugal or cyclone collectors allow the exhaust fumes to enter a silo like structure tangentially causing a vortex. Centrifugal forces then force the particles outward where they collide with the walls and fall under gravity to a collection point under the silo. The gasses then cyclone upward and are released from the top of the silo. This method is relatively effective for particles larger than 5 µm in diameter, removing approximately ninety percent of the particles, and is relatively cheap to implement. However the efficiency drops off dramatically for smaller particles that are of more concern to human health. This makes this technology a good pre-cleaner for one of the next two technologies.

Fabric filtration allows the exhaust fumes to pass through a filter bag which is suspended upside down in a large chamber called a baghouse. A single baghouse may contain thousands of bags. The filtration is mostly performed by the particulates themselves. Some particulates adhere to the inside of the bags creating a fine mesh through which other particulates are filtered and drop out the bottom of the bag. Efficiencies approach 100% for particles as small as 5 µm, and are relatively high for particles as small as 0.01 µm. The are several negative elements to fabric filtration: the bags require regular cleaning to remove build-up of particles; baghouses cannot operate in moist or corrosive environments; they are a potential fire hazard; are expensive; and, use a lot of space. Despite this, their popularity is rising.

Electrostatic precipitators are the most popular form of filtration of particulate matter. Exhaust fumes are passed between two grounded plates. Wires carrying a very high voltage (as much as 100 KV) are placed orthogonal to the flow. The intense electric field causes a corona discharge, which ionizes the gas molecules near the wire. Some of these gas molecules attach themselves to particulate matter causing the particulate matter to be drawn onto a grounded collection electrode. They are removed from the electrode using gravity, rapping or flushing with a fluid. The efficiency of an electrostatic precipitator is a non-linear function of the plate area. Small

increases of efficiency require very large percentage increases in surface area. Efficiencies of 99.9% have been achieved using a plate area measured in tens of thousands of square meters (using parallel plates). It is thus easy to see that electrostatic precipitators are costly and highly space consuming [**1**].

2.3 GLOBAL CLIMATE CHANGE

In 1992, in Rio de Janeiro, the United Nations Framework Convention on Climate Change (UNFCCC) introduced the issue of climate change as a global problem for the first time. Since then world focus has increasingly shifted towards this problem, which is today regarded as the greatest threat to the planet and its inhabitants [**2**].

It is important to understand the difference between climate and weather. Weather is regarded as the current atmospheric conditions and takes into account parameters like temperature, pressure, humidity and rainfall. The weather changes from instance to instance. Climate is the average weather, and until recently was regarded as entirely constant on a scale of tens, hundreds or even thousands of years. The parameters represent the average weather for that particular location and time of year [**3**].

The problem of global climate change simply put, is that the Earth's climate is getting warmer. Even minor changes in climate can have a catastrophic effect on inhabitability of the planet. For example, a 0.1 percent reduction in the energy received from the sun, caused by periodic changes in the Earth's orbit, have been shown to correlate directly to ice ages in the distant past [**1**].

2.3.1 A Simple World Energy Model and the Greenhouse Effect

Recent modelling of climate change is done by splitting the planet up onto a horizontal grid. The interaction of each grid element is then modelled accurately, assuming the knowledge of the boundary conditions and that the climate within each element is constant. This method is known as the fully dynamical general circulation model (GCM) and is highly computing intensive [**3**]. As a result, grid elements are 200 km in the horizontal directions and create a resolution of five times that.

The easiest way to understand global climate from a temperature perspective is with a highly simplified model that equates the amount of energy incident on the Earth, from which a

reflected percentage is subtracted (currently regarded as 31%), with the energy the Earth must radiate if it is considered be a sphere with a uniform temperature. In order for the average energy in the climate to remain constant, the equation must balance. It can be shown, that in order for the equation to balance the Earth's average temperature must be -19 °C, which is 34 °C colder than the actual average temperature of 15 °C [**1**].

The correcting factor to the model is the layer of "insulation" around the planet, which prevents some of the radiation from the planet's surface from escaping to space. This phenomenon is known as the greenhouse effect and is named after the glass greenhouses used by gardeners to create an artificial tropical climate in which to grow plants that require higher temperature and humidity.

The greenhouse gasses, water (H_20), carbon dioxide (CO_2), methane (CH_4), nitrous oxide (N_2O) ozone (O_3), Hydro fluoro compounds (HFC's), Perfluorocarbons (PFC's) and Sulphur hexafluoride (SF_6), insulate the Earth preventing some of the radiation from escaping the atmosphere, reradiating the energy back to the Earth (Figure 2). Of these, water and ozone are not considered to be manmade pollutants, and are not listed as controlled substances in pollution protocols regarding climate change. It is important to note that the energy being emitted from the sun, an extremely hot body, is of a shorter wavelength than the energy radiated from the Earth, a significantly cooler body. This is why the "insulation" allows the incident energy through more readily than the reflected energy. This effectively means that the Earth receives more energy than it transmits, thus increasing its temperature. This increase in temperature causes the Earth to emit more energy until a new equilibrium point is reached at a higher global average temperature.

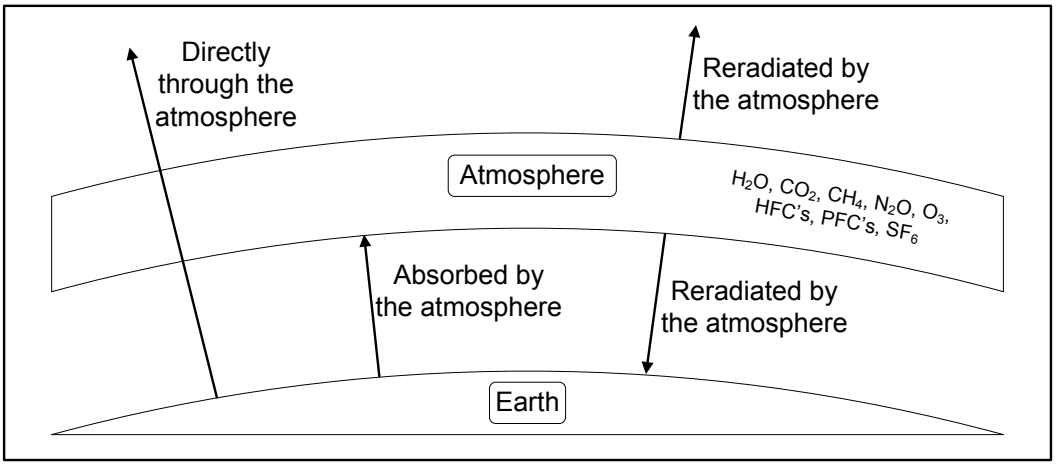

Figure 2 Diagram showing how greenhouse gasses in the atmosphere prevent the Earth from radiating energy directly into space.

Increasing the total amount of greenhouse gasses in the atmosphere adds to this affect and thus increases the global average temperature. Much speculation has been made as to how much temperature increase the planet can withstand without significant adaptation, and how much the concentration of greenhouse gasses would have to increase to cause this change. It is generally accepted that a change larger than 2 °C is not only catastrophic, but also very likely unless emission of greenhouse gasses are reduced significantly.

2.3.2 The Effect of Particulate Matter on Global Warming

The effect of particulate matter in the atmosphere seems to be the subject of some debate. Many sources indicate that the increased energy reflection off the atmosphere caused by particulate matter causes global cooling, and in fact, is mitigating the full impact of the greenhouse effect by up to 40% [**1**]. Other sources, though more recent, say that research indicates that the black carbon, which makes up a considerable percentage of particulate matter, is the second leading cause of global warming [**4**]. Either way, it is clear that the release of particulate matter into the atmosphere is having some impact on the climate.

2.4 SMOKE STACKS

Smokes stacks are the final stage of most industrial combustion processes, and are effectively industrial chimneys that take the form of a tall vertical pipe or channel, often made from steel or reinforced concrete. They were originally designed to enhance the combustion process by creating a draft of air into the combustion zone using the *stack effect* discussed below. At present, the flow of

air into the combustion zone is carefully controlled by forced draught fans and smoke stacks now serve mainly to spread the pollution created by the process over a larger area to comply with government standards.

Smoke stacks vary dramatically from application to application. They can have internal diameters larger than two meters, and vary in height from tens of meters high to over three hundred.

To gain insight into the expected flow rate through smoke stacks, one can examine the property of smoke stacks exploited by earlier combustion processes called the *stack effect.* The stack effect is a phenomenon in gasses that creates a flow proportional to the square root of the height of the stack and the temperature difference between the exhaust gasses and the outside air. Calculating the flow created by the stack effect for a small smoke stack operating at a relatively low temperature would result in a conservative value for the flow rates in smoke stacks, which is required for the modelling of any filtration systems used inside a smoke stack.

The equation below provides an approximation of the volume flow rate of a smoke stack using this thermal draft. The equation neglects frictional resistance and heat losses. It also assumes that the molar mass of the gas inside the stack and the outside air are the same.

$$\Phi = CA\sqrt{2gl\frac{T_i - T_o}{T_i}}, \tag{3}$$

where: Φ is the volume flow rate in $m.s^{-1}$; C is the discharge coefficient usually between 0.65 and 0.7; A is the cross-sectional area in m^2; g is the acceleration due to gravity in $m.s^{-2}$; l is the length of the smoke stack in meters; T_i is the average absolute temperature inside the smoke stack in Kelvin (K); and, T_o is the ambient absolute temperature outside the smoke stack in Kelvin (K).

Hence the flow rate in $m.s^{-1}$ can be given by:

$$\mathrm{q} = \frac{\Phi}{\mathrm{A}} = C\sqrt{2gl\frac{T_i - T_o}{T_i}}, \tag{4}$$

where q is the flow rate in $m.s^{-1}$.

In order to establish the minimum power needed for acoustic filtration in smoke stacks a typical value of a flow rate is needed. It is shown in section 6.3 that higher flow rates result in higher power requirements. For a small smoke stack, 30 m long, operating at 373 K (i.e. steam), with any internal diameter, Equation (4) produces an approximation of 7.3 $m.s^{-1}$. Thus, the flow rate of smoke stacks in general can be conservatively modelled around this value.

3 BACKGROUND TO ACOUSTIC FILTERING

3.1 THE KUNDT'S TUBE APPARATUS

Kundt and Lehmann were the first to describe the acoustic force exerted on small particles (relative to the applied wavelength) suspended in a fluid (eg. spirulina cells in water or carbon in air (smoke)), by an acoustic standing wave [**5**]. This time-averaged force was first used to visualize the wavelength of sound by making acoustic fields visible, such as in the well-known Kundt's tube apparatus. The effective result of this force is to drive a particle to either the pressure node or anti-node of the standing wave. This would allow the observer to see the location of the nodes or anti nodes since the particles would bunch or pile primarily at these locations.

This experiment serves as a good starting point for understanding the basic operating principle of acoustic filters. The apparatus consists of a transparent tube with a sound source coupled to one end and a sound reflecting barrier on the other end (Figure 3). Usual air is used as the fluid medium, but any fluid will do. Some sort of particulate matter is added to the tube, traditionally lycopodium powder (a very fine powder created from the spores of certain club mosses) is used, although in modern demonstrations it is often sawdust or polystyrene foam in various forms.

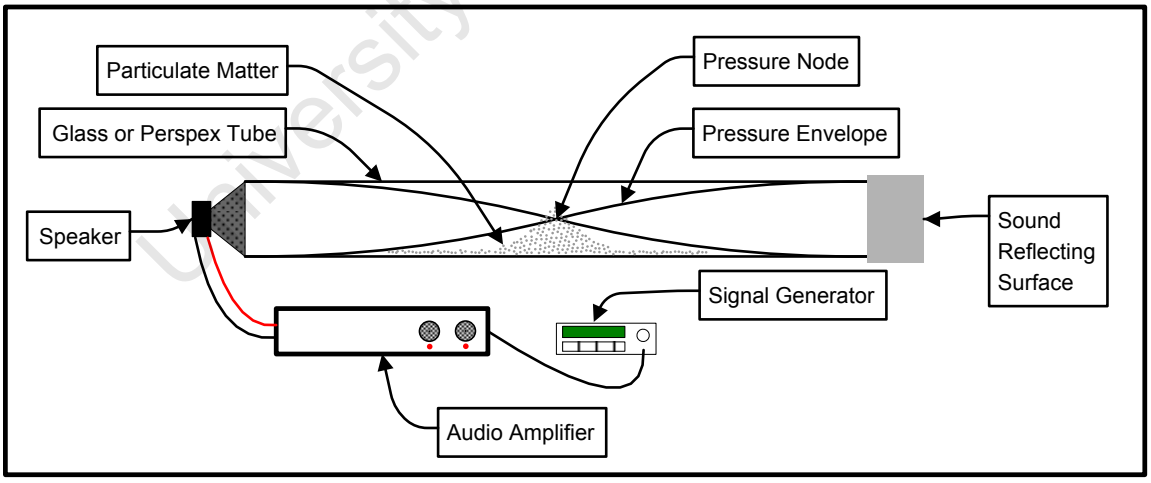

Figure 3 Diagram of the setup of a basic Kundt's tube experiment with a half-wavelength equal to the length of the tube, depicting how particles moves towards the node of the standing wave.

The sound source then applies a single frequency to the tube, in such a way as to set up a longitudinal standing wave in the fluid at one of its resonant frequencies. This is done by using a wavelength of sound such that:

$$N\frac{\lambda}{2} = l, \tag{5}$$

Where: N is any positive integer; λ is the wavelength of sound; and, l is the length of the tube. It must be noted that λ should always be large in comparison with the width of the tube to ensure that the waves created by the source remain planar.

λ can be calculated by the basic relationship of:

$$c_f = \lambda f = \lambda\left(\frac{\omega}{2\pi}\right), \tag{6}$$

where c_f is the speed of sound through the fluid, f is the applied frequency of sound in Hz, which can also be represented as an angular frequency, ω, in rad/s.

After resonance is established, the particulate matter in the tube moves towards the pressure nodes (a point in the standing wave of constant near zero pressure fluctuations). In the case of $N = 1$, the pressure node is in the centre of the tube lengthways.

Conversely, the experiment can be used to establish the speed of sound in the fluid by sweeping the frequency until resonance is observed (particles begin to move to fixed locations). The distance between any two nodes gives $\frac{\lambda}{2}$, and thus, since the frequency is known, c_f can be calculated with Equation (6).

The experiment relies on the quality of the reflective surface. Often when using a poor surface, a proper standing wave cannot be created. A way around that is to use an active reflection by placing a second speaker at the far end of the tube. This way the second speaker, appropriately synchronized in phase and magnitude, produces the same waves as a perfectly reflective surface.

Figure 4 shows how this idea was implemented by the author in practice to move polystyrene foam balls towards the centre of a perspex tube.

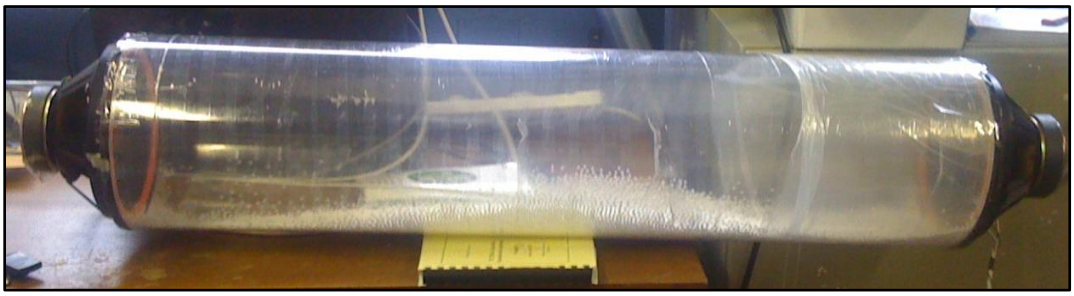

Figure 4 Photo of an active reflection Kundt's tube experiment, depicting polystyrene foam balls moving to a node at the lengthwise centre of the tube.

The sign of the acoustic contrast factor (ACF) indicates whether the force will be in the direction of the nearest pressure node, or the nearest pressure anti-node [**6**]. The ACF is a parameter calculated using the densities and velocities of sound through the fluid and the particle material in question. For example, a water particle in air would be driven to the nearest pressure node, whereas an air bubble in water would be driven to the nearest anti-node.

In more recent years this force has been used in filtering small particles in flowing fluids. While using this acoustic force for filtration may prove to be useful in many applications across diverse media, there is not as yet a significant amount of research being done into practical applications of the technology [**7**,**8**].

3.2 Current Technology and Applications

The backgrounds to several different successfully implemented filter designs are discussed below, of which the most conceptually straightforward being a single half-wavelength filter (Figure 5). The design applies a single half-wavelength standing wave across a cavity through which a mixture flows. As the particles flow through the tube, they are drawn to the centre of the pipe by the acoustic force (in the same manner as in the Kundt's tube apparatus (see section 3.1) except laterally), and flow inline. This results in the fluid towards the exterior of the cavity being clearer and the fluid towards the centre being more densely packed with particles. The clearer fluid can now be filtered out separately through a separate pipe outlet at the end of the filter section [**6**,**9**]. This form of filtering has the advantage of not affecting the actual flow of the fluid by increasing or decreasing the pipe diameter. It is also conceptually simple to implement and model.

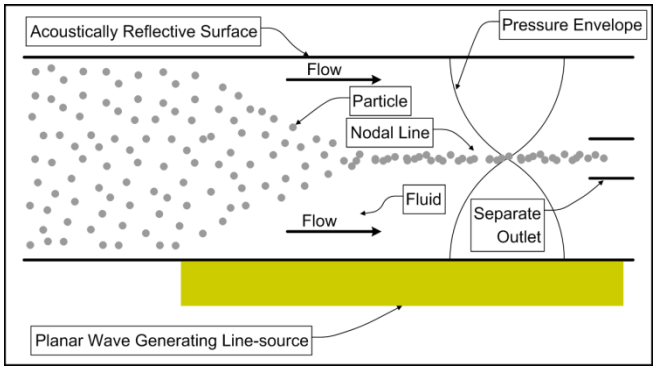

Figure 5 Diagram depicting how a single half-wavelength acoustic filter uses a standing wave to force particles to flow inline so they can be filtered off separately.

The most popular filter design is the h-Shape Separator [**10**,**7**]. Named after the shape of the flow channels, the conceptual operation of the h-Shape Separator is straightforward (Figure 6). A fluid containing suspended particles is allowed to flow through a small pipeline. The pipeline then opens into a larger cavity across which an acoustic force field is exerted. Higher order harmonics of the fundamental resonant mode are applied across the cavity to create multiple pressure nodes running parallel to the flow of the fluid. The particles tend to be 'captured' by the multiple nodes close to the inlet, therefore remaining in the lower portion of the cavity, while the fluid is free to fill the whole cavity. The particles can then be filtered out using a separate outlet to the clearer fluid.

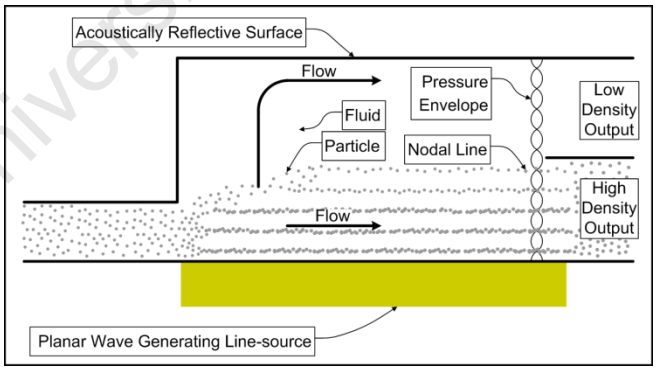

Figure 6 Diagram depicting how the multiple nodes created in an h-shaped separator trap the particles and prevent them from exiting through the low density output.

Much work has been done to optimize the energy density within the cavities of h-filters and to adjust the relative size of the output pipelines for optimization of maximum removal of particles or maximum concentration of particles [**10**,**11**]. A typical h-filter operates at frequencies in the order of

megahertz and has a cavity diameter of 10 mm, operating with fluid flow rates in the order of 100 l/day [**8**].

A drifting resonance field separation device controls the position of the particles rather than simply allowing them to follow a constant trajectory or to move towards a static location [**12**]. Instead of applying the acoustic field directly to the flowing fluid, it is applied through an inactive layer of fluid (Figure 7). This allows the position of the nodes to be controlled by using varying higher order harmonics of the fundamental resonant frequency. By stepping through these modes, a drifting resonant field is created and the particles are swept to one side of the active volume.

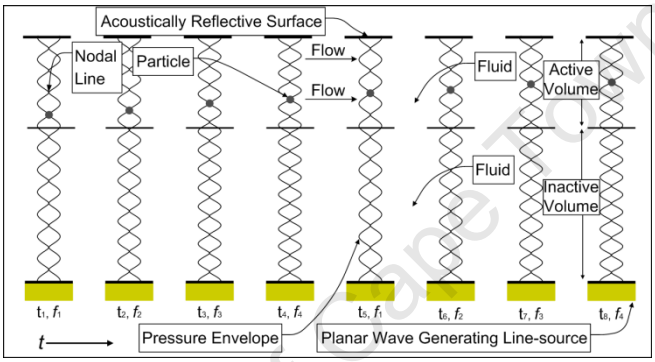

Figure 7 Diagram of the basic operating principle of a drifting resonance field separation device, depicting how progressive harmonics of the fundamental resonant frequency "drift" a particle from one side of the active volume to the other.

While no significant work has been done using acoustic forces to filter particles from gaseous media directly, some research has been done to aid with the filtration of smoke particles from industrial processes. The group of Gallego-Juarez has implemented several designs to agglomerate particles within a process to increase their average size, and thus improve the filtration efficiency of electrostatic filters further on in the process. The design uses a special stepped plate resonator capable of creating massive sound pressure levels in air at frequencies of about 20KHz [**13**].

Applying a high power signal to a particulate mixture has the effect of vibrating the particles. By optimizing the applied frequencies for a particular particle radius, maximum relative displacement between the particles can be obtained. This increases the number of collisions between particles and thus the particles begin to agglomerate or coagulate increasing the particles size and making them more likely to be filtered by a mechanism further along in the process. For a particle radius between 1 µm and 2 µm, a frequency of 20KHz is optimal [**14**].

4 DESIGN OF A "TEST CONCEPT" DIFFUSION CHAMBER ACOUSTIC FILTER

It is shown in section 2 above that the particulate matter, specifically the black carbon, released from the burning of fossil fuels is hazardous to human health and to the world at large. It is also shown that effective means of mitigating these emissions are expensive and space consuming. A new design with a potentially lower cost and significantly lower space requirements would be desirable by the industry. It has been suggested that using acoustic force fields to filter the carbon particles from air would be a possible application of acoustic filtering [**7**,**8**]. Thus, a useful situation for such a design would be to remove the particulate matter being released into the atmosphere by industrial smoke stacks.

Designing the filter to fit within the smoke stack itself would ensure that no additional space is needed and the design could be easily retrofitted. Furthermore, and acoustic filter would present no impedance to the flow, and thus not affect the combustion process itself.

This section outlines the design of a diffusion chamber acoustic filter (DCAF) to mimic the two factors thought to be the most influential in the design of an acoustic filter for use on industrial smoke stacks: having an even distribution of particles over the cross-section of the flow; and, having a large (meters, not millimetres) cross-section over which to filter.

4.1 OPERATING PRINCIPLE

The mechanical design of the test rig depends significantly on the mode of operation of the filter. Several filter operation mechanisms have been put into practice and are outlined in section 3.2. While some of the designs show advantages in terms of effectiveness, simplicity was the strongest motivating factor to use a single half-wavelength filter. The single half-wavelength filter has strong similarities to the setup of the Kundt's tube apparatus (outlined in section 3.1) which had already been implemented, and thus it is expected that following this route would be most time efficient. It would also conceivably allow for easier implementation in a smoke stack scenario.

Since particulate gasses are not practical to work with, small balls of polystyrene foam approximately 2 mm in diameter are used to represent the particles. This is practical because they

are easy to store, and the effectiveness of the filter will be easily observed, as in the Kundt's tube apparatus.

The operating principle of the DCAF is the same as that described in Figure 5. The particles (polystyrene balls) first pass through a diffuser to distribute them evenly over the cross-section of flow and then fall through the filter under gravity. Allowing gravity to drive the flow of particles is analogous to the upward flow of particles in a real smoke stack environment. Smoke stacks typically have diameters of one to two metres (section 2.4). Using a cavity 1 m meter across means that, in accordance to Equation (5), the frequency of operation would be approximately 171.5 Hz (given that the speed of sound in air is 343 $m.s^{-1}$). This is well within the range of bass speakers that are readily available.

4.2 MECHANICAL DESIGN

The mechanical design was separated into several different stages, each performing one of four functions: diffusion; speaker mounting; reflective channel; and support. Each stage can be slotted onto any other stage, which allows for any of the stages to be replaced without affecting adjacent stages; for the order of the stages to be easily changed; and, for new stages to be easily placed into the system. Construction in 6 mm MDF Supawood allows the design to be rigid, reflective to sound, easy to manufacture and light to transport.

The main function of the diffuser stage is to cause the polystyrene to fall uniformly over the cross-section of flow. It is more important that the particles are uniform over the longer dimension than the shorter dimension, since the acoustic force will be exerted over the length. Figure 8 shows the design of the diffuser with a longitudinal funnel which spreads the polystyrene evenly. Additional shelf slots allow further diffusion gratings to be put in place. Results showed that these were not necessary for even distribution. A perspex panel slotted into the front side of the diffuser allows the user to observe the behaviour of the particles, and to gain access to the inside of the stage.

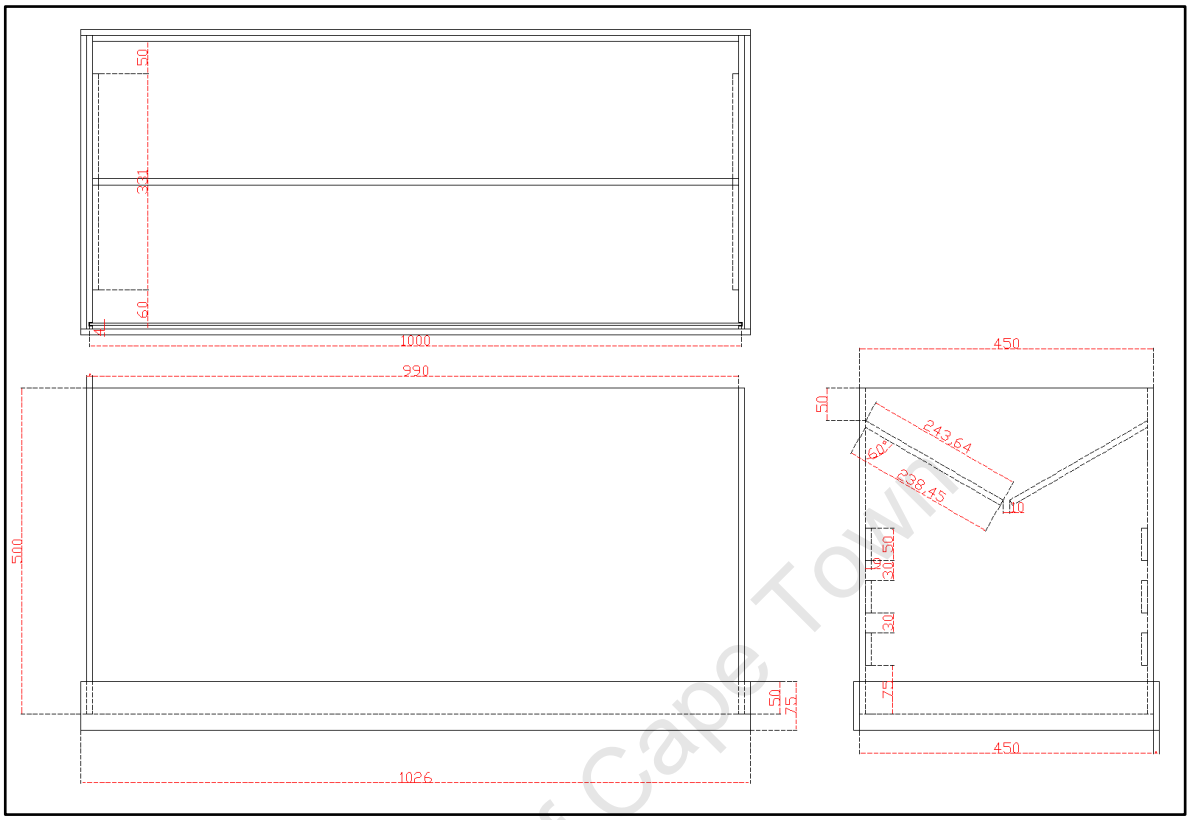

Figure 8 Mechanical drawing showing the design of the diffuser stage used for evenly spreading polystyrene foam balls inside the testing rig. All dimensions in millimetres.

The speaker mounting stage allows for two speakers to be placed opposite each other to create an active pressure standing wave (see section 3.1) (Figure 9). A passive pressure standing wave can be set up by only driving one of the speakers. This stage also has a perspex window for the reasons stated above. Several speaker stages can be placed on top of each other to increase the length across which the acoustic force is applied and to increase the amount of acoustic energy applied to the system.

Placing multiple sound sources in a single cavity could result in pressure cancellations that produce unwanted nodes. The author modelled the scenario of three speaker mounting stages mounted consecutively with two speakers each. The model shows how the sound energy compounds slightly and does not cause deconstructive interference producing unwanted pressure nodes (Figure 10).

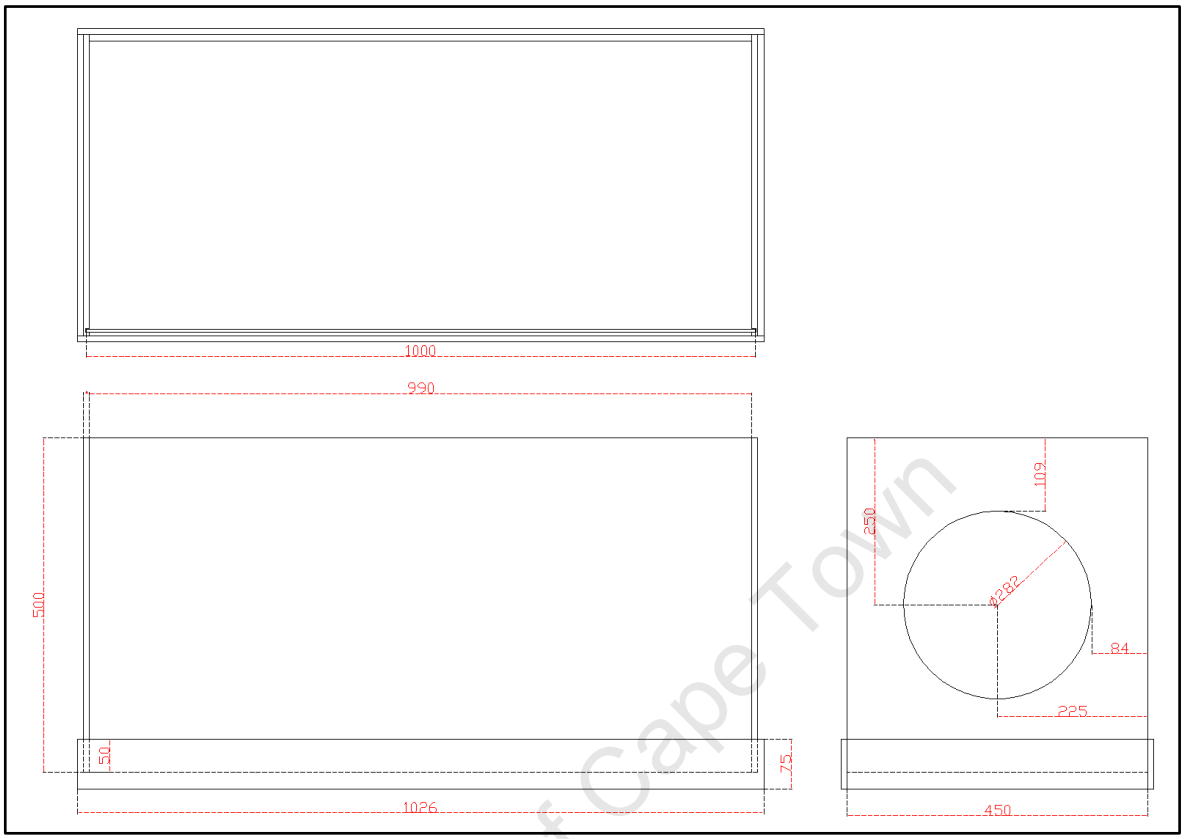

Figure 9 Mechanical drawing showing the design of the speaker mounting stage used to apply a pressure standing wave across the longer dimension of diffusion chamber acoustic filter. All dimensions in millimetres.

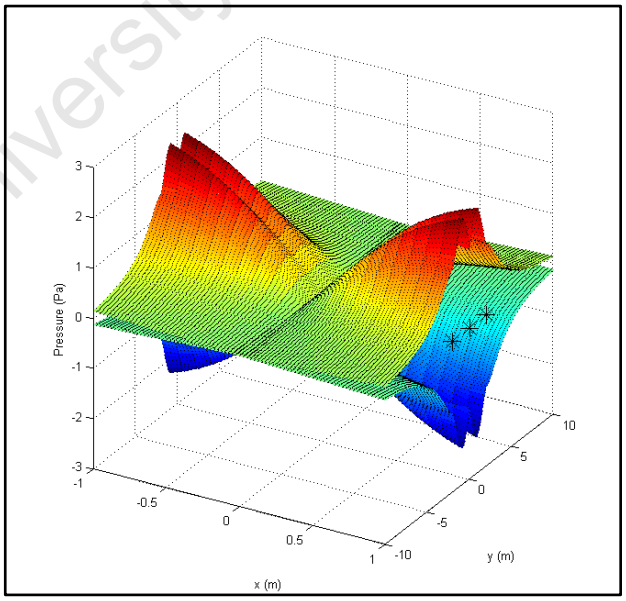

Figure 10 Plot showing the pressure envelope created by six point sound sources, three on each end, placed one half-wavelength apart, represented by stars. The pressure envelope is shown not to cause deconstructive interference producing unwanted nodes in the filtering area. Each sound source is modelled as producing a maximum of 1 Pa.

The reflective channel stage is designed to increase the length of the rig. This is used either to allow the polystyrene to reach terminal velocity before entering the sound field or to show how a section of the channel that does not have a sound source will resonate with energy that is reflected through the channel. This stage also has a perspex window for the reasons stated above.

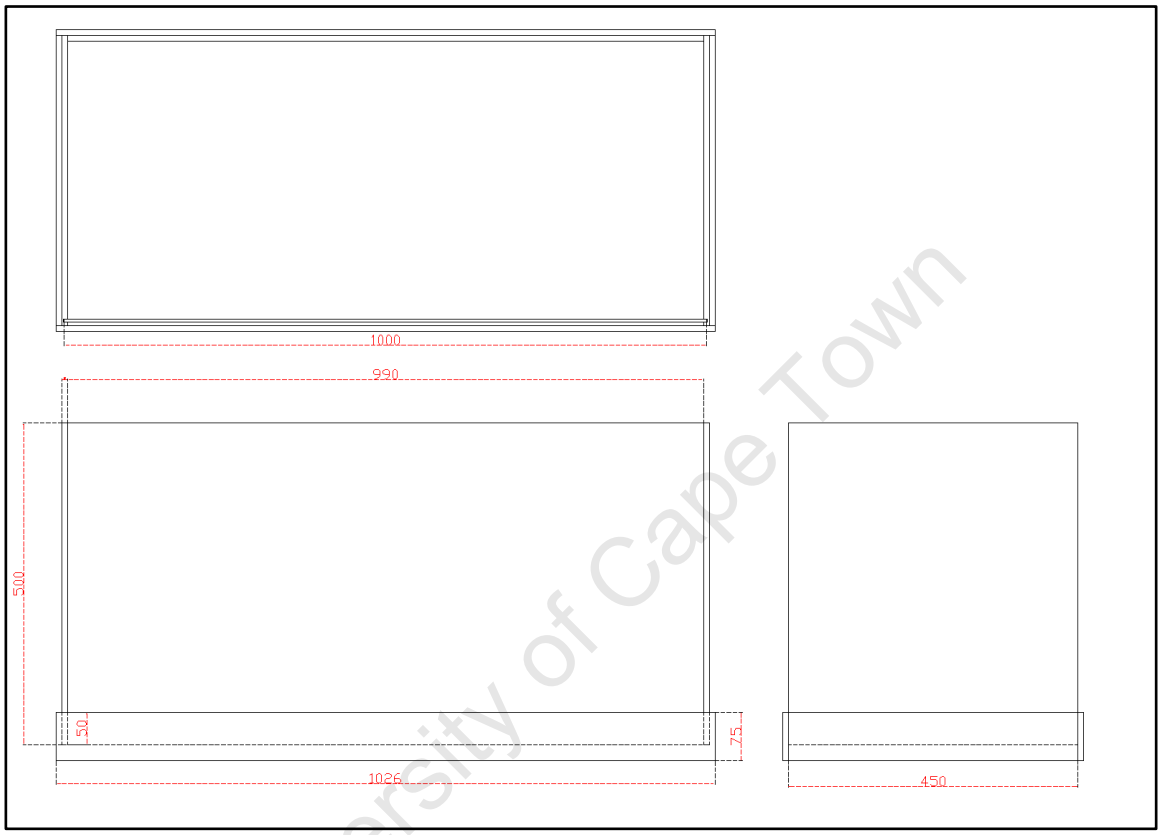

Figure 11 Mechanical drawing showing the design of the reflective channel stage used either to allow the polystyrene to reach terminal velocity before entering the sound field or to show how a section of the channel that does not have a sound source will resonate with energy that is reflected through the channel. All dimensions in millimetres

The support stage provides the rig with legs to raise it off the ground allowing the polystyrene balls to be collected easily. Figure 12 shows the final construction of three of the stages mentioned above: the diffuser stage; the speaker mounting stage; and, the support stage.

Figure 12 Photo showing the final construction of three stages of a test rig for the design of an acoustic air filter for use on smoke stacks. The stages shown are: the diffuser stage (top), the speaker mounting stage (middle) and the support stage (bottom).

4.3 OBTAINING RESONANCE

In order to obtain resonance, an exact half-wavelength of sound must be applied to the cavity across its longer dimension. To do this the speaker must be driven with a frequency such that:

$$f = \frac{c_f}{2}, \tag{7}$$

given that λ is 2 m for a cavity 1 m in length. Until now we have assumed that the speed of sound through air, c_f, is constant. In reality c_f changes with temperature, pressure and humidity and thus differs from day to day. In order to obtain resonance easily on a daily basis the final design would either have to regularly establish the speed of sound using a known distance and a pulse echo method or a phase measurement method, or dynamically adjust to ensure that a half wavelength is always applied.

A phase-lock-loop circuit was implemented to drive the speaker amplifier to ensure a constant phase angle of 180 degrees across the cavity. The circuit (Figure 13) measures the phase angle between the two ends of the cavity using two microphones. If the phase angle is too low, the driving frequency in increased. If the phase angle is too high, then the driving frequency is decreased.

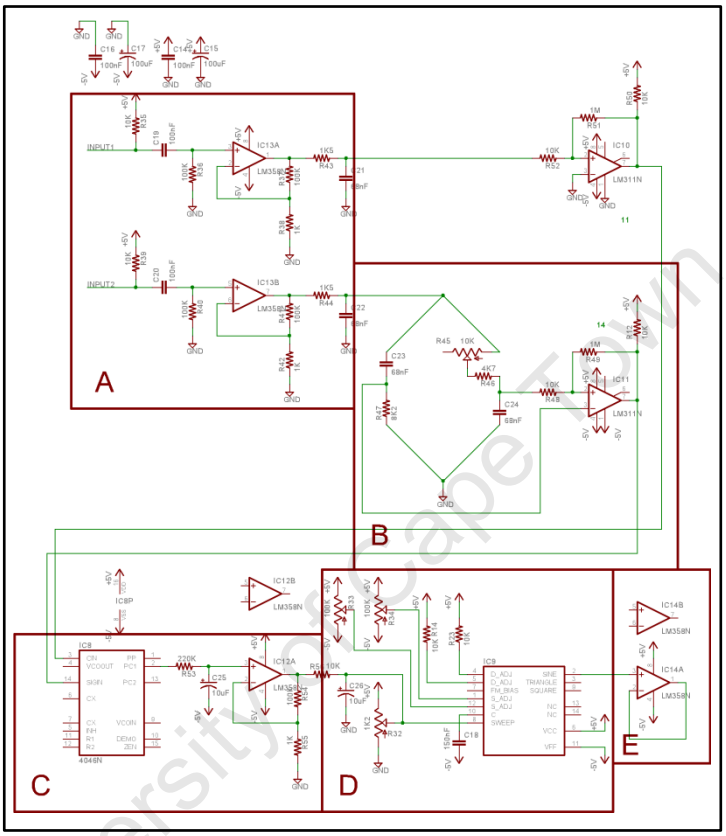

Figure 13 Schematic of a Phase lock loop design for automatically establishing acoustic resonance in a cavity using two microphones. (A) Two input buffers from two standard resistive microphones. (B) Universal 90 degree phase shifter as signal conditioning before the phase detector to allow for zero point tracking. (C) Standard xor phase detector with a low pass filter output. (D) Voltage to frequency converter produces a sine wave output based on the phase difference. (E) Output buffer before the signal is fed into the audio amplifier.

The circuit was shown to track successfully a phase angle of 180 degrees over a wide range of potential cavity distances for a speaker in free space. However, tracking was not successfully implemented inside the test rig cavity. This prompted an investigation into the waveform existing inside the cavity at the frequency at which resonance was expected.

By moving a microphone in the plane of the standing wave over a 5 cm × 5 cm grid, and measuring the phase relative to the driving signal on the speaker and the amplitude, a picture of the waveform can be generated and even animated since the frequency is known. The measurement of 171 points (9 by 19) over the grid resulted in the waveform shown in Figure 14. The waveform shows that the

expected half-wavelength standing wave was not forming at all, and in fact, what appeared to be significantly shorter wavelengths were present. This is even more apparent when the image is animated.

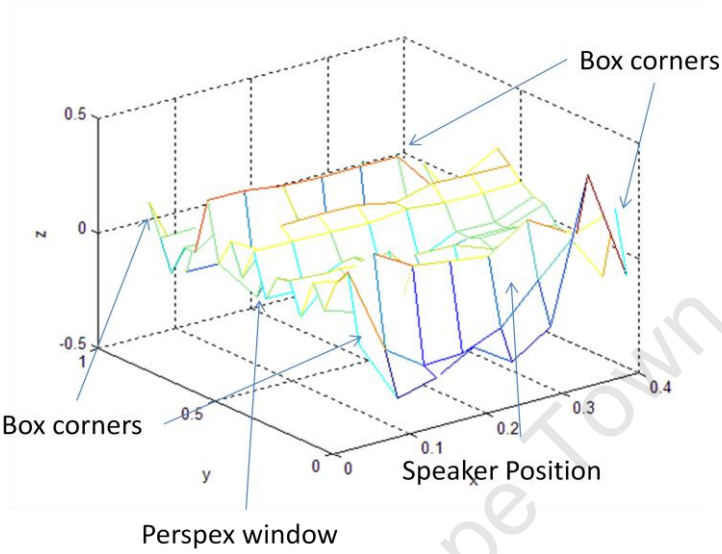

Figure 14 Waveform generated inside the speaker mounting stage. The plot shows multiple peaks possibly representing higher frequencies than the applied signal.

After further investigation, this phenomenon was thought to show one of the false assumptions of the design. At such low frequencies, 6 mm MDF Supawood does not reflect sound. Without going into detailed theory of acoustic impedance, it suffices to say that nothing short of a thick brick wall will reflect such low frequencies. The waveform is thought to be the sum result of multiple reflections off the walls of the laboratory in which the experiment was conducted.

Consequently, none of the energy put into the system would resonate inside the cavity. This not only meant that reflective resonance was impossible, but also that more energy would be required to achieve the same amplitude of sound. Without rebuilding the cavity in thick metal or concrete, using an active standing wave with two speakers was the only means of achieving a half-wavelength standing wave.

4.4 Measurement of the Acoustic Force

Using both speakers, an active standing wave with an amplitude of approximately 120 dB re. 1×10^{-12} W.m^{-2} (the threshold of human pain in hearing) was achieved. In order to measure the acoustic force, thought to be a maximum at one-quarter wavelength or at the cavity

walls, a pendulum method was used. A single polystyrene ball hung on a fine nylon thread (known as invisible thread, used in professional magic tricks) was suspended from the diffuser stage. Despite the large magnitude of the acoustic field, no notable deflection was seen in the pendulum.

Calculating the force required to deflect such a pendulum 1 mm when suspended 0.6 m is straightforward. First, the mass of a single polystyrene ball and the thread must be known. This was measured using a calibrated digital scale used for measuring small amounts of chemical compounds. The mass of a typical polystyrene foam ball was found to be 1.3×10^{-6} Kg, supposedly accurate to 0.1×10^{-6} Kg, while the mass of the thread was found to be negligible in comparison.

Figure 15 shows how the horizontal component of the tension must cancel with the acoustic force and that the vertical component of the tension must cancel with the weight of the ball in order for the system to be in equilibrium.

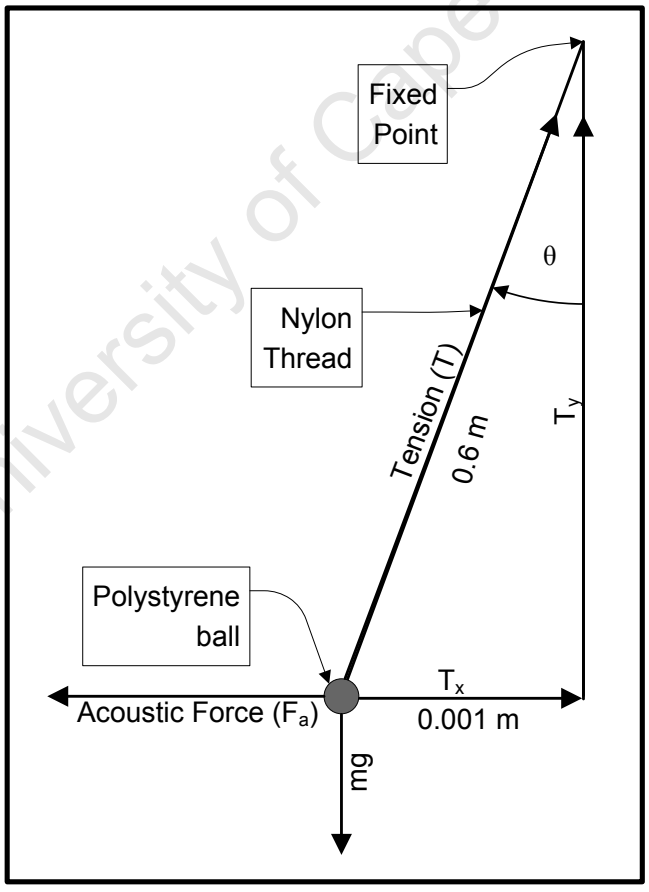

Figure 15 Force diagram for a pendulum deflected by 1 mm showing the balance of forces when the pendulum is in equilibrium. Not to scale.

Calculating the actual magnitude of the forces, since $T_y = mg$:

$$T_y = T\cos(\theta) = T\cos\left(\arcsin\left(\frac{0.001}{0.6}\right)\right) = mg, \tag{8}$$

where: m is the mass of the particle and is 1.3×10^{-6} Kg; g is the acceleration due to gravity and is 9.81 m.s^{-2}; and, θ is the angle the pendulum makes with the vertical. Hence:

$$T = \frac{mg}{\cos\left(\arcsin\left(\frac{0.001}{0.6}\right)\right)}. \tag{9}$$

Therefore we can calculate T_x by:

$$T_x = T\sin(\theta) = \frac{mg}{\cos\left(\arcsin\left(\frac{0.001}{0.6}\right)\right)}.\frac{0.001}{0.6}, \tag{10}$$

and since for equilibrium $T_x = F_a$, F_a can be given by:

$$F_a = \frac{1.3 \times 10^{-6}.9.81}{\cos\left(\arcsin\left(\frac{0.001}{0.6}\right)\right)}.\frac{0.001}{0.6} = 21.26 \times 10^{-9}\ N \tag{11}$$

The calculated force has no meaning unless the magnitude of the pressure wave required to create such a force is known. It is clear that a greater understanding of the theory of the acoustic force is required in order to understand why the pendulum failed to deflect. This is covered in detail in section 5 below. The calculation of the required pressure amplitude for a deflection of 1 mm is carried out in section 5.3.

5 CALCULATION OF THE ACOUSTIC RADIATION FORCE

It is shown in section 4 above that the intuitive understanding of the acoustic radiation force gained from the Kundt's tube apparatus is not sufficient to produce a working design of an acoustic filter. In order to properly model the nature of the force and the power requirements in the filter design the background theory to the force must be developed.

At this stage, it is useful to define several parameters, many of which are similar and can cause much confusion. Each parameter will be defined again when they appear first in application, but it is best that the differences be explicitly spoken of here.

Two different particles are spoken of in the sections to follow. A *fluid particle* is a discrete block of the fluid medium through which a planar sound or pressure wave travels. It does not refer to a molecule of the substance, but rather just an infinitesimally small block of the fluid assuming the fluid to be completely continuous. A *particle* (no "fluid" before it) is simply an impurity in the fluid. It can be aerodynamically approximated by a sphere having different material properties to the fluid in which the pressure wave travels.

Both the fluid and the particle have their respective speed of sounds and densities. Explicitly, c_f and c_p are the velocities of sound through the fluid medium and the particle respectively, and ρ_f and ρ_p are the densities of the fluid medium and the particle respectively. The density is the mean density of the substance and not the instantaneously altered density of the material when propagating a pressure wave.

When a pressure wave is incident on a fluid particle the fluid particle is displaced from its equilibrium position. There is no net movement of the fluid particle, it simply vibrates around its equilibrium point. The fluid particle's instantaneous one dimensional deviation from its equilibrium position is denoted by ξ. The instantaneous velocity of a fluid particle is denoted by v and is not to be confused with the velocity of a particle, V.

Finally, for adiabatic gasses, the following equation shows the relationship between ξ along the dimension of propagation of the wave, x, and the magnitude of the pressure fluctuation, p, above and below the mean pressure [**13**]:

$$p = -\rho_f c_f^2 \frac{\partial \xi}{\partial x}, \tag{12}$$

p is not to be confused with the average pressure of the fluid usually denoted by P. It is simply the difference between the instantaneous pressure and the mean pressure of the fluid medium.

5.1 THE ACOUSTIC RADIATION FORCE EQUATION

Yisioka et al. [**14**,**15**,**16**] and later Gor'kov [**17**] presented the first analysis of the acoustic force exerted on a single small compressible sphere (relative to the wavelength). Previous analysis had considered a simpler scenario of non-compressible spheres [**18**]. Gor'kov gives the time-averaged force on a single, small, compressible sphere in an arbitrary sound field as:

$$\boldsymbol{F} = -\nabla\left(\frac{2}{3}\pi R^3\left[\frac{\overline{p^2}}{\rho_f c_f^2} - \frac{\overline{p^2}}{\rho_p c_p^2} - \frac{3\rho_f(\rho_p - \rho_f)}{2\rho_p - \rho_f}\overline{v^2}\right]\right), \tag{13}$$

where: $\overline{\mathrm{p}^2}$ is mean square of pressure; $\overline{v^2}$ is the mean square of the fluid particle velocity; R is the particle radius; ρ_f and ρ_p are the densities of the fluid medium and the particle respectively; and, $\mathrm{c_f}$ and $\mathrm{c_p}$ are the velocities of sound through the fluid medium and the particle respectively.

The acoustic force equation in this form is difficult to understand and apply. The following derivation was performed by the author to allow the acoustic force to be applied easily to various modelling situations.

Since only the pressure and the fluid particle velocity are spatially dependant, Equation (13) can be rewritten for a wave along a single dimension x as:

$$F = -\frac{2}{3}\pi R^3\left(\left[\frac{1}{\rho_f c_f^2} - \frac{1}{\rho_p c_p^2}\right]\frac{\partial \overline{p^2}}{\partial x} - \left[\frac{3\rho_f(\rho_p - \rho_f)}{2\rho_p - \rho_f}\right]\frac{\partial \overline{v^2}}{\partial x}\right). \tag{14}$$

In this form, the equation shows how the magnitude of the force is proportional to the volume of the particle and is spatially dependent on the gradient of the pressure and fluid particle velocity waves.

Equation (12) can be rearranged and integrated to make ξ the subject of the formula:

$$\xi = \int \frac{-p}{\rho_f c_f^2} . dx \tag{15}$$

where p denotes the pressure fluctuations of the fluid medium and ξ is the displacement of a fluid particle from its equilibrium position. A compression standing wave in a fluid can be represented as two waves of the same amplitude travelling in opposite directions [**19**]:

$$p(x,t) = \mathrm{A}\cos(\omega t - kx) + A\cos(\omega t + kx), \tag{16}$$

where $p(x,t)$ denotes the pressure at any given point in space and time along a single dimension x, ω is the angular frequency of the wave, the combined amplitude of the two waves is given by $2 \times A$ and k is the wave number which is equal to $\frac{\omega}{c_f}$. Thus by substituting Equation (16) into Equation (15):

$$\xi = \frac{-A}{\rho_f c_f^2} \int [\cos(\omega t - kx) + \cos(\omega t + kx)] . dx, \tag{17}$$

$$= \frac{-A}{\rho_f c_f^2 k} [\sin(\omega t + kx) - \sin(\omega t - kx) + K], \tag{18}$$

where K is an arbitrary constant of integration and is not to be confused with k, the wave number. The instantaneous fluid particle velocity of the standing wave can now by calculated using:

$$v(x,t) = \frac{\partial \xi}{\partial t} = \frac{\partial \left(\frac{-A}{\rho_f c_f^2 k} [\sin(\omega t + kx) - \sin(\omega t - kx) + K] \right)}{\partial t} \tag{19}$$

$$= \frac{A}{\rho_f c_f} \cos(\omega t - kx) - \frac{A}{\rho_f c_f} \cos(\omega t + kx), \tag{20}$$

where $v(x,t)$ denotes the fluid particle velocity at any given point in space and time along a single dimension x.

Finally the required parameters for the acoustic force equation can be calculated by taking the partial derivatives of the pressure and fluid particle velocity with respect to x:

$$\frac{\partial \overline{p^2}}{\partial x} = -8A^2 k \sin(2kx), \tag{21}$$

and

$$\frac{\partial \overline{v^2}}{\partial x} = \frac{8A^2 k}{\rho_f^2 C_f^2} \sin(2kx). \tag{22}$$

By substituting Equation (21) and Equation (22) into Equation (14) it can be shown that for a planar standing wave, in a single dimension, in air, that Equation (13) can be reduced to:

$$\boldsymbol{F} = A^2 \omega C \sin(2kx), \tag{23}$$

where:

$$C = -\frac{4}{3}\pi R^3 \frac{-5\rho_p^2 c_p^2 + 2\rho_p c_p^2 \rho_f + 2\rho_f c_f^2 \rho_p + \rho_f^2 c_f^2}{c_f^3 \rho_f c_p^2 \rho_p (2\rho_p + \rho_f)}. \tag{24}$$

5.2 Measurement of Material Parameters

Before the magnitude of the acoustic force can be calculated, all the parameters of Equation (23) and Equation (24) must be known. This thesis aims to use the acoustic radiation force in a smoke stack scenario, thus parameters from this environment should be used to calculate the acoustic force. In section 2.2.1, carbon particles with a diameter between 2 µm and 4 µm are the most dangerous to humans. Therefore, modelling of carbon graphite particles with a radius of 1 µm results in a worst case scenario as smaller particles are harder to filter.

Polystyrene foam balls must also be modelled in order to understand the behaviour of the test rig in section 4. The speed of sound through and density of air and carbon is easily referenced. The speed of sound and the density of polystyrene foam balls must both be measured experimentally.

In order to measure the density of the polystyrene with reasonable accuracy a bulk volume of polystyrene balls can be weighed inside a container. Obviously, the volume of the container is much

greater than the total volume of the polystyrene inside the container due to all the air spaces. For spheres of a constant radius in a container considerably larger than the volume of one sphere, the total average volume as a ratio to the volume of sum of all the spheres is given by the packing factor $\frac{\pi}{3\sqrt{2}} = 0.74$ [**20**]. Appendix A shows the mass data taken several times for several different volumes of polystyrene balls, and, a check using the same scale to measure the density of water. The density of a polystyrene ball was finally calculated by:

$$\rho_p = \frac{Total\ Mass - Mass\ of\ the\ Beaker}{Total\ Volume \times 0.74} \tag{25}$$

The results of several iterations of the experiment showed little variation with an average density given as approximately 18 Kg/m^3.

The speed of sound through a single polystyrene ball is very difficult to measure. An approximate value can be obtained by sending an acoustic pulse down the length of a polystyrene foam rectangular prism (Figure 16) and measuring the time taken for the signal to propagate down the length.

Figure 16 Photo of a rig used to measure the speed of sound through a rectangular polystyrene prism. An ultrasonic transducer transmits a pulse on one end of the prism and an oscilloscope measures the amount of time taken for the pulse to travel to a second transducer at the other end of the prism

The speed of sound can be calculated by:

$$c_p = \frac{l}{t_p}, \tag{26}$$

where: c_p is the speed of sound through the particle material, in this case polystyrene; l is the length of the prism; and, t_p is the time taken for the sound wave to propagate the length of the prism. The piezoelectric transducer used has an extra terminal to output the deflection of the transducer so that the measured signal directly correlates to an acoustic wave in the material

(Figure 17). This implies a direct phase relationship between the measured transmitted and received pulses that allows a very accurate time interval to be measured (Figure 18).

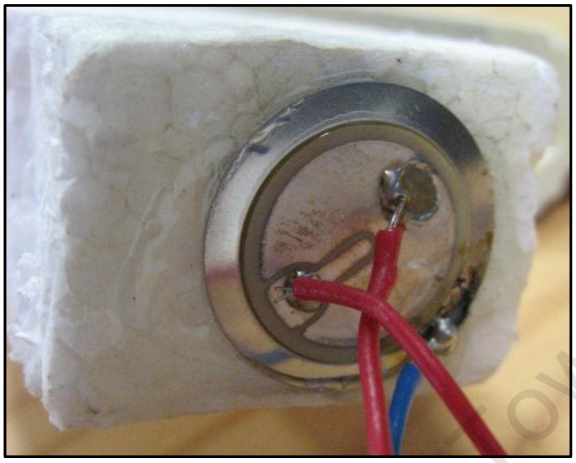

Figure 17 Photo of the piezoelectric transducer used to measure the speed of sound through polystyrene. The third terminal allows the actual deflection of the transducer to be measured when it is driven.

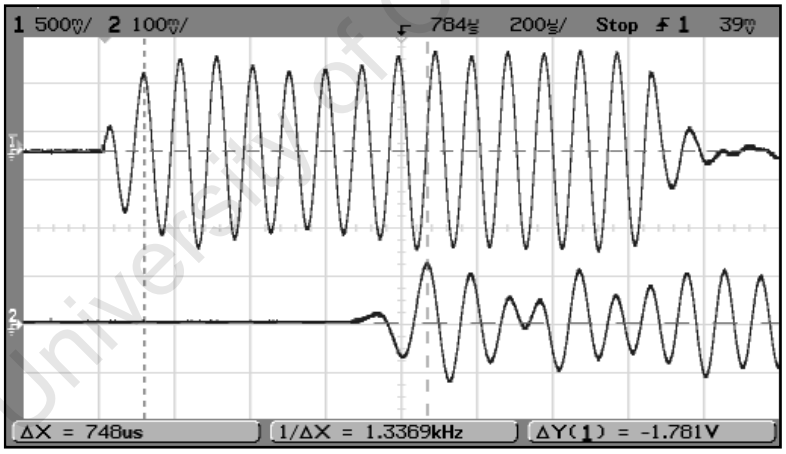

Figure 18 Graph of the transmitted and received ultrasonic pulses in a polystyrene foam prism. The length of time taken for the pulse to propagate is inversely proportional to the speed of sound through the material. Trace 1 is the transmitted pulse and trace 2 is the received pulse.

The average result of performing this experiment yielded a speed of sound through polystyrene of approximately 600 $m.s^{-1}$. This result is probably higher than the real value since the polystyrene block is slightly more compressed than a single ball, but is accurate enough to serve as a guide for modelling.

The following table can be drawn up denoting the material parameters needed by Equation (23) for the modelling of the acoustic radiation force:

Table 1 Table of properties of air, graphite and polystyrene foam used to calculate the acoustic force on a particle.

Substance	**Density – ρ ($kg.m^{-3}$)**	**Speed of Sound - c ($m.s^{-1}$)**	**Particle Radius -R (m)**	**C ($m^3.s.kg^{-1}$)**
Air	1.21	343	N/A	N/A
Graphite	2200	3800	1×10^{-6}	2×10^{-25}
Polystyrene Foam	18	600	1×10^{-3}	2×10^{-16}

The magnitude of the acoustic radiation force can now be calculated along the axis of a half-wavelength pressure standing wave. Figure 19 shows the one-dimensional force exerted on a polystyrene ball with a radius of 1 mm for a reference intensity of 1 $W.m^{-2}$ or 120 dB re. 1×10^{-12} $W.m^{-2}$, which is the threshold of acoustic pain in humans. For a half-wavelength of one meter in air, $\omega = 171.5$ Hz. The graph clearly shows that particles to the left of the centre experience a positive force pushing them towards the centre, and particles to the right of the centre experience a negative force, also towards the centre. This explains why particles in the Kundt's tube apparatus move towards the centre of the tube when a half-wavelength standing wave is applied.

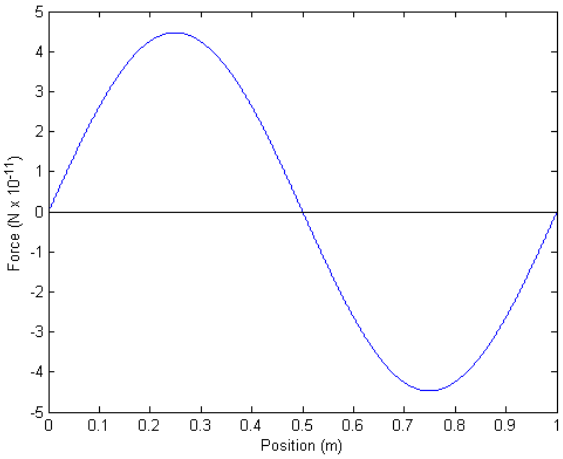

Figure 19 Graph of the one dimensional force exerted on a small particle of polystyrene foam across a single half-wavelength acoustic standing wave, showing that particles to the left of the centre experience a positive force pushing them towards the centre, and particles to the right of the centre experience a negative force, also forcing particles towards the centre.

5.3 Calculation of the Acoustic Intensity Required for a Pendulum Deflection of 1 mm

The acoustic intensity needed to create a maximum force of 21.26×10^{-9} N and deflect the pendulum discussed in section 4.4 by 1 mm can now be calculated. Rearranging Equation (23):

$$A = \sqrt{\frac{\mathrm{F}}{\omega C \sin(2kx)}}, \tag{27}$$

where, as stated above, the amplitude of the standing wave is given by $2 \times A$. Since $\sin(2kx)$ has a maximum value of 1, and acoustic intensity, I, is given by:

$$I = \frac{(amplitude)^2}{2\rho_f c_f}, \tag{28}$$

the minimum acoustic intensity can be given by:

$$I = \frac{4.\frac{\mathrm{F}}{\omega C}}{2\rho_f c_f}. \tag{29}$$

Equation (29) gives the required acoustic intensity as 475 W.m^{-1} or 147 dB re. 1×10^{-12} W.m^{-2}. This intensity is considerably higher (more than four hundred times higher) than that exerted in the DCAF in section 4.4, and exceeds the capabilities of the test rig. The theory explains why the pendulum failed to deflect, and certainly indicates that the power requirements of such a filter would be large. However, the failure of the pendulum to deflect does not necessarily show that the filter, in its dynamic state, using carbon particles, will need as much power. To answer this question the filter in a realistic dynamic situation must be modelled.

6 MODELLING OF SMOKE STACK FILTRATION

The efficiency of a single half-wavelength acoustic filter is dependent on how effectively the impurities are forced to a single location within the filter. Since the acoustic force varies with space (Figure 19), the behaviour of a particle depends on the dimensions of the specific scenario.

6.1 THEORETICAL CONFIGURATION

This study focuses on addressing the pollution caused by smoke stacks, and thus the theoretical scenario is largely based on typical operating parameters of an industrial smoke stack.

For this study, a simplified model of smoke stack filtration is put forward, much the same as the diffusion chamber acoustic filter design in section 4. The smoke stack is assumed to have a rectangular cross-section of 1 m $\times$ 0.5 m as depicted in Figure 20. A rectangular cross-section is used for simplicity, but the result can easily be extended to the circular case.

A single half-wavelength standing wave is excited along the longer dimension, again for simplicity of design and concept, with the goal of driving particles to the centre. This creates a thickened layer of impurities in the centre that can be filtered out separately to the clearer gas towards the outside as in Figure 5.

The region in the centre of the longer dimension where particles could be filtered out separately will be referred to as the *filtration zone*. The region where particles are to be moved out of the flow, and towards the filtration zone, will be referred to as the *target zone*. The particles in the target zone must be moved into the filtration zone before exiting the filter for effective filtration to occur. The amount of time taken for a particle on the outside of the target zone to move into the filtration zone will be referred to as τ_{max}. Arbitrarily, the goal will be to move approximately 90% of the particles into 10% of the cross-section. The 10% dead band is created because the low magnitudes of acoustic force at the outside of the smoke stack (Figure 19) would cause very large τ_{max} values and distort the measure of the effectiveness of the filter. The target zone thus extends from 0.05 m from the edges to 0.05 m from the centre, and the filtration zone extends 0.05 m in both directions outwards from the centre.

A smoke particle is modelled as carbon (graphite) with a particle radius of 1 µm. A model of polystyrene foam would more readily be verified by experiment, thus particles of polystyrene foam, 2 mm in diameter, are also considered.

The model assumes two sound sources creating the opposing sound waves, described in Equation (16), creating an active standing wave. Each source contributes half of the required power. This is done as the resonant characteristics of a chimney or filter design are variable. The Q of the system allows one to introduce losses and possible chamber gains. This model can only be applied directly if the acoustic quality factor (Q) of the chimney is 1, as in the case of the diffusion chamber acoustic filter. In order to take into account the Q of the system, the power required should be divided by the Q to obtain the total power needed.

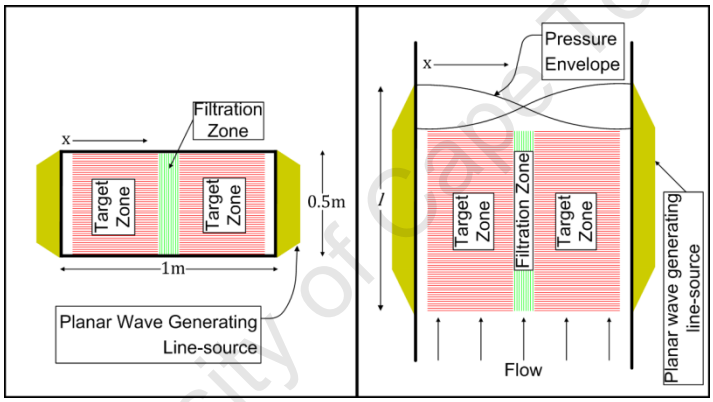

Figure 20 Diagram of modelling parameters for acoustic filtration over a large cross-section. The side view on the right shows how the acoustic field is applied over a fixed length.

6.2 Modelling of Particle Motion

To properly model the effectiveness of a given filter design the motion of a particle in any location within the filter must be accurately modelled.

6.2.1 Finding a Closed Form Solution for the Particle Motion

Finding a closed form solution for the particle position as a function of time would be the most efficient way to analyse a filter design, since simulations would only need a few simple arithmetic calculations to establish whether particles have moved to the required location inside the filter within the allotted time. To find a particle's position as a function of time given its acceleration as a function of displacement is a simple process.

Firstly, Equation (23) must be adapted to represent the acceleration, a, of a particle:

$$a(x) = \frac{\boldsymbol{F}(x)}{m} = \frac{A^2 \omega C \sin(2kx)}{m}, \tag{30}$$

where m is the mass of the particle and is calculated for a spherical particle from its density and radius. Given that [**21**]:

$$V.dV = a.dx, \tag{31}$$

where V is the velocity of the particle, not the fluid particle velocity of the medium as in Equation (13), and substituting in Equation (30) and integrating we get that:

$$\int_{V_0}^{V} V.dV = \int_{x_0}^{x} a(x).dx, \tag{32}$$

or

$$V^2 = V_0^2 + 2\int_{x_0}^{x} a(x).dx. \tag{33}$$

The author from here executes the derivation through to produce the particle position as a function of time. Solving the integral:

$$\int_{x_0}^{x} a(x).dx = \int_{x_0}^{x} \frac{A^2 \omega C \sin(2kx)}{m}.dx = \left| \frac{-A^2 \omega C}{2km} \cos(2kx) \right|_{x_0}^{x} \tag{34}$$

$$= \frac{-A^2 \omega C}{2km} \cos(2kx) - \frac{-A^2 \omega C}{2km} \cos(2kx_0). \tag{35}$$

Assuming a particle entering the filter would have no initial velocity in the direction of the acoustic force, can set V_0 can be set to 0 and therefore:

$$V(x) = \sqrt{\frac{-A^2 \omega C}{km} [\cos(2kx) - \cos(2kx_0)]} \tag{36}$$

Given:

$$V = \frac{dx}{dt}, \tag{37}$$

and substituting in, rearranging and integrating to give:

$$\int_{x_0}^{x} \frac{dx}{V(x)} = \int_{0}^{t} dt \tag{38}$$

or

$$t = \int_{x_0}^{x} \frac{dx}{V(x)} = \int_{x_0}^{x} \frac{dx}{\sqrt{\frac{-A^2\omega C}{km}[\cos(2kx) - \cos(2kx_0)]}} \tag{39}$$

which would, assuming this integral can be found, give time as a function of displacement and therefore, by rearranging the equation, give displacement as a function of time. Even though A, ω, C, K, m and x_0 can be treated as constants for a given simulation scenario, this integral has no closed form solution. The best method for solving the motion of the particle would then be to use some form of approximation method.

6.2.2 The Fourth Order Runge-Kutta Method

Since no closed form solution can be found (section 6.2.1) even for the simplest analysis of the acoustic forces on the particle, an accurate simulation method is needed. The Runge-Kutta methods, created by the German mathematicians C. Runge and M.W. Kutta in the early 1900's provide a robust method for approximating the solutions to systems of first order differential equations.

The method attempts to find approximations to the solution of [**22**]:

$$y' = f(t, y) \quad a \leq t \leq b \quad y(a) = \alpha, \tag{40}$$

by splitting the time interval up into N finite segments where each segment has a length of h, i.e.:

$$t_i = a + ih \qquad i = 0,1,2 \dots, N, \tag{41}$$

where the length of h is given by:

$$h = \frac{b - a}{N}, \tag{42}$$

and finding an approximation to the real solution at each of these points. The higher the value of N the greater the accuracy, and also the greater the number of iterations needed to find the final answer.

It is useful to define a function that represents the solution to $y(t)$, but differentiates itself from the true solution since it is an approximation:

$$\omega_i \approx y(t_i) \quad for\ i = 0,1,2 \dots, N. \tag{43}$$

The *fourth order* Runge-Kutta method is commonly used and offers a high degree of accuracy while still limiting the amount of steps required. Instead of presenting, in general terms, the full algorithm of the fourth order Runge-Kutta method adapted for a system of differential equations, the system presented by the motion of a particle in a viscous fluid exposed to an acoustic radiation force will be used as both an example and demonstration.

Firstly, the system of first order differential equations needs to be defined. Since a lengthy simulation will be performed regardless, a more complex analysis can be done than that done when searching for the closed form solution above. Several other forces, besides the acoustic radiation force act on the particles within the filter, such as Konig and Bjerknes forces [**23**]. These forces will not be taken in to account in this analysis. The Stokes drag force affects the motion of the particle significantly and must be taken into account. The drag force is the chief form of energy loss in the particle and is that which prevents the particle from oscillating around the node perpetually like a mass on a lossless spring.

The Stokes drag force is given as [**12**]:

$$\boldsymbol{F_d} = -6\pi\mu R\boldsymbol{V}, \tag{44}$$

where μ is the dynamic viscosity of the fluid medium, air in this case, which has a value of about 1.78×10^{-5} Pa.s.

Combining Equation (23) and Equation (44) the acceleration of the particle, a, is now:

$$a = \frac{\boldsymbol{F}(x) + \boldsymbol{F_d}(\boldsymbol{V})}{m} \tag{45}$$

Figure 21 shows a state diagram depicting how the variables representing the motion of a particle exposed to an acoustic field within a viscous fluid can be related to each other through integration. Division by S denotes integration with respect to time.

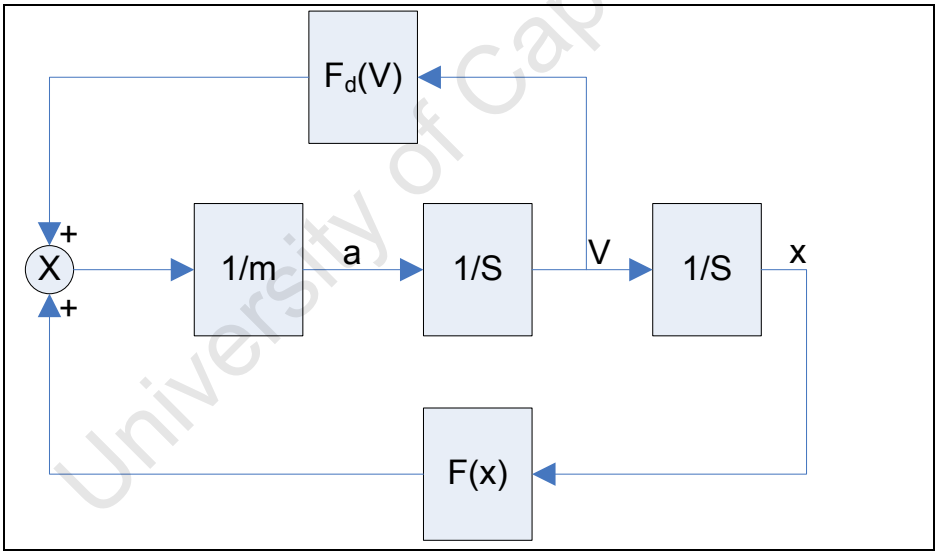

Figure 21 State diagram depicting how the variables representing the motion of a particle exposed to an acoustic field within a viscous fluid can be related to each other through integration.

From Figure 21, the system can be expressed as a set of two first order differential equations in terms of position (x) and velocity (V) where:

$$\dot{x} = V \qquad \text{and} \tag{46}$$

$$\dot{V} = \frac{\boldsymbol{F}(x) + \boldsymbol{F}_d(V)}{m}. \tag{47}$$

The Runge-Kutta method requires initial values for both variables, x and V and for the limits of t to be predefined. These values will be assigned during simulation and can be represented here as, x_0, V_0 and $a \leq t \leq b$. Since there are two states we now define two approximation functions:

$$\omega_{x,i} \approx x(t_i) \qquad \text{and} \tag{48}$$

$$\omega_{V,i} \approx V(t_i) \quad for\ i = 0,1,2 \ldots, N \tag{49}$$

Thus, the algorithm builds the solution for $\omega_{x,i+1}$ and $\omega_{V,i+1}$ from the previous known point or approximation thus:

$$\omega_{x,0} = x_o, \quad \omega_{V,0} = V_0 \tag{50}$$

$$K_{1,x} = h\omega_{V,i} \tag{51}$$

$$K_{1,V} = h\frac{\boldsymbol{F}(\omega_{x,i}) + \boldsymbol{F}_d(\omega_{V,i})}{m} \tag{52}$$

$$K_{2,x} = h(\omega_{V,i} + \frac{1}{2}K_{1,V}) \tag{53}$$

$$K_{2,V} = h\frac{\boldsymbol{F}\left(\omega_{x,i} + \frac{1}{2}K_{1,x}\right) + \boldsymbol{F}_d\left(\omega_{V,i} + \frac{1}{2}K_{1,V}\right)}{m} \tag{54}$$

$$K_{3,x} = h(\omega_{V,i} + \frac{1}{2}K_{2,V}) \tag{55}$$

$$K_{3,V} = h\frac{\boldsymbol{F}\left(\omega_{x,i} + \frac{1}{2}K_{2,x}\right) + \boldsymbol{F}_d\left(\omega_{V,i} + \frac{1}{2}K_{2,V}\right)}{m} \tag{56}$$

$$K_{4,x} = h(\omega_{V,i} + K_{3,V}) \tag{57}$$

$$K_{4,V} = h\frac{\boldsymbol{F}(\omega_{x,i} + K_{3,x}) + \boldsymbol{F}_d(\omega_{V,i} + K_{3,V})}{m} \tag{58}$$

$$\omega_{x,i+1} = \omega_{x,i} + \frac{1}{6}(K_{1,x} + 2K_{2,x} + 2K_{3,x} + K_{4,x}) \tag{59}$$

$$\omega_{V,i+1} = \omega_{V,i} + \frac{1}{6}\left(K_{1,V} + 2K_{2,V} + 2K_{3,V} + K_{4,V}\right) \tag{60}$$

for $i = 0,1,2 \ldots, N$.

This may look complicated, but every step is a simple arithmetic equation that builds from the previous step, with each iteration calculating four K's and an approximation to the solution for each of the two dependent variables. Error analysis for the method allows the step size, h, to be dynamically changed during simulation to allow a maximum step size, while staying within the limits of local and global truncation errors. This allows for a faster simulation time, which can become highly beneficial for simulations requiring high accuracy. Even though this method has many more steps per iteration than other methods, like the well known Euler's Method, its superior accuracy allows for significantly fewer iterations to be taken while maintaining the required accuracy.

This method can easily be implemented in code and is in fact already implemented by Matlab using a variable step method that allows error tolerances to be set.

Using this set of first order differential equations a fourth order Runge-Kutta approximation can accurately simulate the position of the particle over time. Figure 22 shows the particle trajectories for both graphite (R = 1 µm) and polystyrene foam (R = 1 mm) calculated using this Runge-Kutta approximation. It demonstrates the relative intensities required for a τ_{max} of about four seconds for both materials.

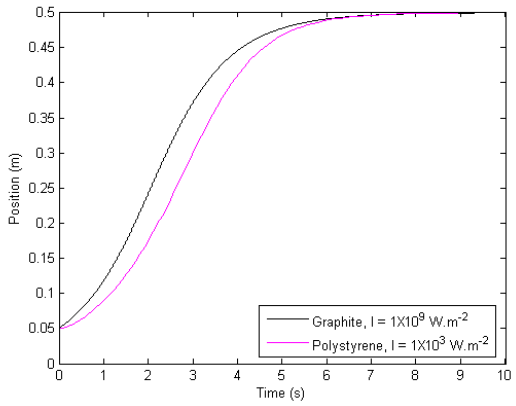

Figure 22 Particle position against time for a single particle starting from rest on the outside of the target zone for both graphite (I = 1×10^9 W.m^{-2}) and polystyrene foam (I = 1×10^3 W.m^{-2}).

6.3 MODELLING OF POWER REQUIREMENTS

It is easiest to consider a section of the smoke stack with length l as part of the filter with the assumption that any sound that escapes this section, be it down the length of the smoke stack or in another form of dissipation, does not contribute to the forcing function. For effective filtration to occur the maximum settling time is given as:

$$\tau_{max} = \frac{l}{q}, \tag{61}$$

where q is the flow rate of the fluid in m.s^{-1}.

It was observed in simulation that τ_{max} and acoustic intensity have an inverse relationship for τ_{max} values above a threshold (Figure 23). For very high values of intensity, this relationship is no longer true, as τ_{max} becomes almost constant with respect to changes in intensity. Operating in this region of the graph is energy inefficient since further increasing the power offers no gains in the effectiveness of the filtration. A stepping pattern in τ_{max} was observed for intensities above this threshold. This is caused by the particle oscillating around the set point through the filtration zone. There are various critical intensities which mark the point at which the particle requires an additional oscillation before finally remaining within the filtration zone, thus creating a sudden increase in the τ_{max} value.

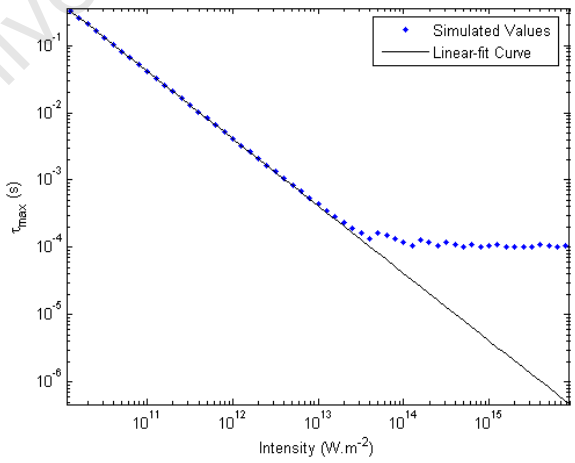

Figure 23 Graph depicting the inverse relationship between τ_{max} and acoustic intensity for graphite, and the deviation above the linear-fit curve for high intensities.

For τ_{max} values above this threshold value, the required intensity for a given τ_{max} is given by:

$$\frac{\mathrm{I}}{\mathrm{I_r}} = \frac{\tau}{\tau_{\max}}, \tag{62}$$

where I is acoustic intensity in W.m^{-2}, and τ is the settling time corresponding to a reference intensity $\mathrm{I_r} = 1$ W.m^{-2} (i.e. the y-axis intercept of Figure 23).

It was shown in simulation that the relationship holds true for polystyrene foam with a different value of τ. The values of τ for graphite and polystyrene foam are $4.1 \times 10^9 s$ and $4.4 \times 10^3 s$ respectively.

The acoustic power required with a Q of 1 is:

$$P = I \times A = I \times 0.5 \times l, \tag{63}$$

where A is the area orthogonal to the wave direction.

By combining Equation (61), Equation (62) and Equation (63), it can be shown that the minimum power for effective filtering is given by:

$$P = \frac{\tau\, \mathrm{I_r}}{\frac{l}{q}} \times 0.5 \times l = q\frac{\tau\, \mathrm{I_r}}{2}. \tag{64}$$

This gives the minimum acoustic power needed for effective filtering in a smoke stack with the conservative flow rate of 7.3 m.s^{-1} established in section 2.4, as approximately 15 GW and approximately 16 KW for graphite and polystyrene foam respectively. It is also important to note that the final power is independent of l.

For comparison, the required power for a τ_{max} of two seconds for polystyrene foam was calculated for a longitudinal standing wave in a tube with diameter of 5 cm as in a typical Kundt's tube apparatus (section 3.1). The tube inherently has a Q of approximately 2 because of the near perfect reflection off one of its ends, and the minimal losses through the sides of the tube. The power for this setup can be given by:

$$P = \frac{\tau \, \mathrm{I_r}}{\tau_{max}} \times \mathrm{A} \times \frac{1}{\mathrm{Q}} = \frac{\tau \, \mathrm{I_r}}{2} \times \frac{\pi(0.05)^2}{4} \times \frac{1}{2}. \tag{65}$$

The required acoustic power according to the developed model was computed as 2.16 W, which is in the correct order of magnitude for this type of apparatus. This suggests that the model is reasonably grounded in reality.

6.4 Discussion of Results

6.4.1 Total Power Required for Effective Filtration

The minimum power required for effective filtration of carbon particles with a conservative flow rate of 7.3 m.s^{-1} in this arrangement is given as 15 GW. It can be seen through the relationships developed above that mildly changing some of the basic parameters of the arrangement will not reduce this number sufficiently for it to enter the realm of feasibility.

While it is true that raising the Q of the system will reduce the required power proportionally, a large Q is not expected due to the losses incurred due to the cavity having open ends. Furthermore, the efficiencies of high power acoustic transducers in this range are very low, and serve to increase dramatically the amount of electrical power required by the system.

6.4.2 Optimizing the Length of the Filter

Figure 23 coupled with Equation (64) above represent a very significant result. It demonstrates that the amount of power needed for a given flow rate as a function of l is constant until reaching a particular threshold. Reducing l further forces τ_{max} into the non-linear region of Figure 23.

If one were to ignore the Stokes drag force, this result would be expected. Applying a smaller acoustic force over a longer flow distance would have the same affect on τ_{max} as a larger acoustic force over a shorter flow distance. Hence, the total power would remain constant.

Accounting for the Stokes drag force, one would expect that increasing l would cause a reduction in the necessary average velocity of the particle and thus a reduction in the energy lost through drag. Equation (64) simply shows that for velocities below a certain threshold, the reduction in velocity caused by further increasing l would be insignificant in terms of saving energy.

An examination of Figure 23 in the non-linear region shows that for a given τ_{max} a larger intensity is needed than that given by the linear-fit curve. Hence, it is more energy efficient to use a filter with a longer l in order to increase the required τ_{max} (further into the linear region) than it would be to operate in the non-linear region of the graph.

7 MODELLING FOR PARTICLES WITH DIFFERENT PARAMETERS

The result discussed in section 6.4.2 indicates that the methods developed have implications in optimizing the design of filters for other applications. Widening the scope of the analysis to include particulate matter with different particle radii, speed of sounds, and densities would allow the model the versatility to be applied to other filter designs.

7.1 MODELLING OF PARTICLES WITH A DIFFERENT RADIUS

Modelling until this point has assumed a constant particle radius. In reality, particulate matter is produced in a variety of particle sizes ranging from 1 µm to 10 µm in diameter. An analysis of the behaviour of τ_{max} in relation to particle size would give an indication of how effective a particular filter design would be on particles of different radii.

Figure 24 shows the relationship between particle radius and τ_{max} for three different intensities. By projecting up from the horizontal axis onto one of the three graphs τ_{max} for that intensity and particle radius can be obtained. It can be seen that for a particular radius there is a threshold intensity, where further increasing the intensity would not result in decreasing τ_{max}.

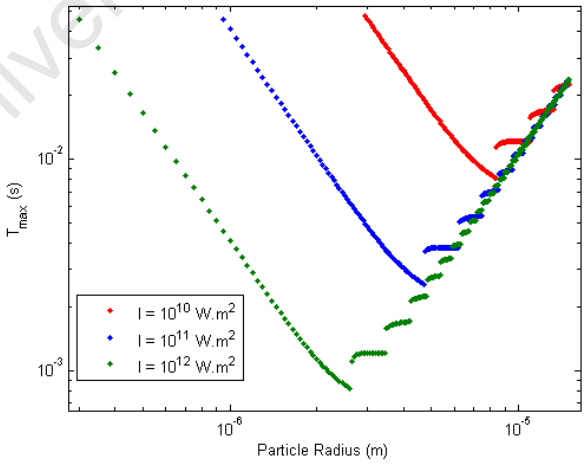

Figure 24 Graph of particle radius versus particle settling time for graphite showing how for a given particle radius the setting time becomes constant with increasing intensity above a threshold.

This threshold point is simply the representation of the same threshold seen in Figure 23. The discontinuities in the graph are again cause by the particle's oscillation through the filtration zone as discussed in section 6.3. A plot of the relationship between the threshold intensity for different radii can be developed in simulation (Figure 25).

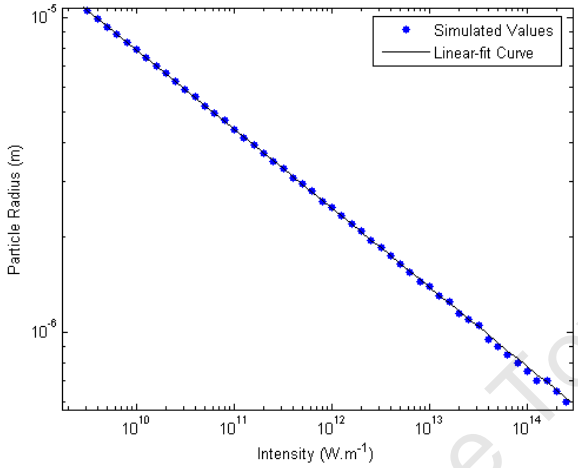

Figure 25 Graph showing the relationship between threshold intensity and particle radius.

The plot shows that for a given material, graphite in this case, the threshold intensity can be given by:

$$I = \alpha R^{\beta} \tag{66}$$

Where α and β are specific to the material, and in the case of graphite are 5.1×10^{11} and -3.98 respectively. Being able to calculate the threshold intensity allows a design to ensure that when filtering particles of variable sizes, the filter operates within the constant power region of Figure 23 for all particle sizes.

7.2 MODELLING FOR PARTICLES OF DIFFERENT MATERIALS

The scaling constant C from Equation (23) is a function of particle radius and of the speed of sound and density of the particle, if the fluid medium is a constant. Modelling the dependence of settling time on the speed of sound and density of the particle gives an understanding of how a filter would behave for a range of materials.

Figure 26 shows the settling time plotted for values of speed of sound and density that cover most solid materials. The graph shows how the material parameters have little effect on the settling time. The graph indicates that except for materials with a very low density (below 50 $kg.m^{-1}$), the modelling developed in sections 6.3 and 7 apply to most solid materials with little error.

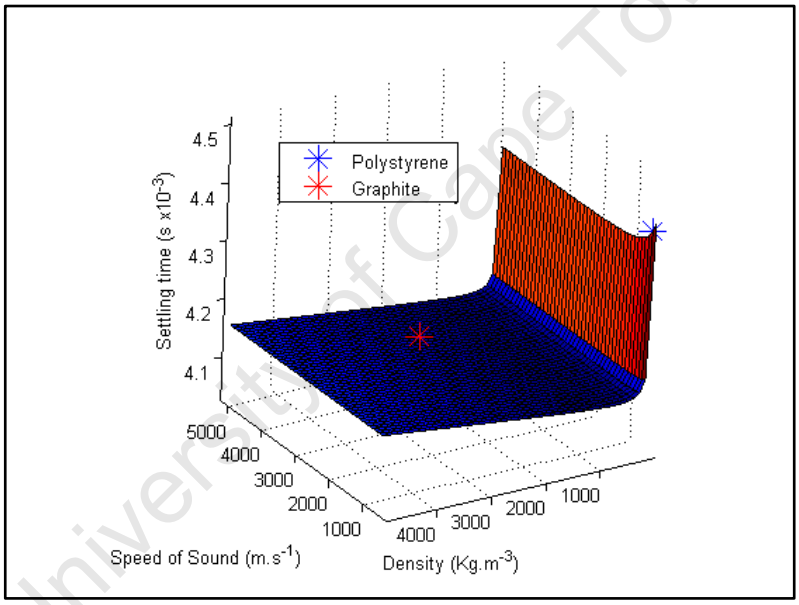

Figure 26 Three-dimensional plot showing the settling time for most solid materials while holding the intensity constant. The graph shows how for most materials settling time varies very little with either density or speed of sound.

8 CONCLUSIONS

8.1 EFFECTIVE EMISSION CONTROLS A NECESSITY

It is known that the emissions created by the combustion of hydrocarbons in industrial processes, transportation and the production of electricity are hazardous to human health and contribute toward global climate change. Proper control of these emissions is imperative to prevent premature deaths, health problems and damage to the ecology of the planet.

Particulate matter, mostly produced in power stations and exhausted through smoke stacks, is one of these pollutants. Effective means of mitigating particulate matter is currently expensive and space consuming. A new, cheaper and less space consuming technology for the mitigation of particulate matter emission would be beneficial to the industry.

8.2 LARGE POWER REQUIREMENTS CAUSE ACOUSTIC FILTERING OVER A LARGE CROSS-SECTION TO BE INFEASIBLE

It has been shown that acoustic filtering is a working form of filtration implemented in several designs filtering across small cavity widths. It has been shown that the power needed to scale this idea up to large cavity widths, such as in the industrial smoke stack environment is unfeasibly large. The conclusion only applies to the configuration applied in this thesis, and thus implies that if acoustic filtration is to be applied to environments with large volume flow rates, a new configuration of acoustic filtration is needed.

The amount of power needed is so large, that several power stations would be needed to power the acoustic filter on just one of the smoke stacks in one of those power stations.

8.3 EFFICIENCY OF ANY ACOUSTIC FILTER CAN BE OPTIMIZED

It has been shown that proper design of the combination of the wave front length and acoustic intensity allows the power consumption of the filter to be optimal. If the filter is operated in its optimal region the amount of power required for effective filtration to occur is not a function of the applied wave front length, but rather a function of the flow rate in an acoustic filter. It has been

shown how the relationship between the minimum acoustic wave front length and the required acoustic intensity can be explicitly expressed for a given particle radius and material.

It has also been shown that for a particular particle radius and material a minimum achievable settling time can be calculated. Applying acoustic intensities larger than that required to achieve this settling time would have no further affect on the settling time and simply waist the extra power added, thus making the filter inefficient. This threshold value can be given as an explicit function of particle radius for a given material.

It has also been shown how the design tools developed are applicable to a wide range of materials. The methods developed have used a particular filter design and scenario, but apply equally well when using any acoustic filter design where the goal is to move a particle to a particular location within a particular time frame.

8.4 FUTURE WORK

The analysis presented in this thesis provides a strong argument as to why this work should be discontinued. The analysis does however fall short of presenting a complete study on the topic, and thus several areas, should they be investigated further, may prove to be beneficial and worthwhile.

In particular, the analysis presented here should be accompanied with a full design of an acoustic resonator taking into account boundary conditions and the real Q of such a resonator. The analysis should also include the nonlinear effects of air caused by the high sound pressure levels required for such a filter, and examine their effect on a particle's motion. Finally, and most importantly, the filtering mechanism should be changed to a more complex system. The low frequencies and long distances required by a single half-wavelength acoustic filter foreseeably contribute towards the high power required for effective filtration, and thus a different configuration may address these problems.

9 REFERENCES

1. Masters, G. M.: Introduction to environmental engineering and science 2nd edn. Prentice Hall (1998)
2. Winkler, H.: Climate change mitigation negotiations, with an emphasis on options for developing countries., An Environment and Energy Group publication (2008)
3. Stone, D.: Predicted climate change for years to come and implications for disease impact studies. Rev. sci. tech. Off. int. Epiz, 27 (2) (2008)
4. Jacobson, M. Z.: Strong radiative heating due to the mixing state of black carbon in atmospheric aerosols. Nature 409, 695-697 (2001)
5. Kundt, A., Lehmann, O.: Longitudinal vibrations and acoustic figures in cylindrical columns of liquids. Annalen der Physik und Chemie 153, 1-11 (1874)
6. Goddard, G., Kaduchak, G.: Particle concentration in a line-driven tube. J. Acoust. Soc. Am. 117, No. 6, 3340-3347 (2005)
7. Benes, E., Gröschl, M., Nowotny, H., Bohm, H., Radel, S., Houser, C., Power, J. B., Lowe, K. C., Briarty, L. G., Davey, M. R.: The ultrasonic h-shape separator: harvesting of the alga spirulina platensis under zero-gravity conditions. Proc. World Cong. of Ultrasonics, 1631-1638 (2003)
8. Benes, E., Gröschl, M., Nowotny, H., Trampler, F., Keigzer, T., Bohm, H., Radel, S., Gherardini, L., Hawkes, J. J., Konig, R., Delouvroy, C.: Ultrasonic separation of suspended particles. IEEE Ultrasonics Symposium, 649-659 (2001)
9. Hawkes, J., Coakley, W. T., Groschl, M., Benes, E., Armstrong, S., Tasker, P. J., Nowotny, H.: Single half-wavelength ultrasonic particle filter: Predictions of the transfer matrix multilayer resonator model and experimental filtration results. J. Acoust. Soc. Am. 111, No 3, 1259-1266 (2002)
10. Bohm, H., Briarty, L. G., Lowe, K. C., Power, J. B., Benes, E., Davey, M. R.: Quantification of novel h-shaped ultrasonic resonator for separation of biomaterials under terrestrial gravity and microgravity conditions. Biotechnol. Bioeng. 82, No 1, 74-85 (2003)
11. Hawkes, J., Gröschl, M., Benes, E., Nowotny, H., Coakley, W. T.: Positioning particles within liquids using ultrasonic force fields. Proc. Forum Acusticum (2002)
12. Handi, B., Gröschl, M., Trampler, F., Benes, E., Woodside, S. M., Piret, J. M.: Particle trajectories in a drifting resonance field separation device. Proc. Int. Congr. Acoust., Acoust. Soc. of Am. 3, 1957-1958 (1998)

13. Riera, E., Gallego-Juarez, J. A., Mason, T. J.: Airborne ultrasound for the precipitation of smokes and powders and the destruction of foams. Ultrasonic Sonochemistry 13, 107-116 (2006)
14. Hueter, T. F., Bolt, R. H.: Sonics: Techniques for use of sound and ultrasound in engineering and science. John Wiley and Son, INC. (1955)
15. Kinsler, L. E., Frey, A. R.: Fundamentals of Acoustics 2nd edn. John Wiley and Sons Inc. (1950)
16. Yosioka, K., Kaisima, Y.: Acoustic radiation pressure on a compressible sphere. Acustica 5, 167-173 (1955)
17. Hasegawa, T., Yosioka, K.: Acoustic radiation force on a solid elastic sphere. J. Acoust. Soc. Am. 46, 1139-1143 (1969)
18. Hasegawa, K., Yosioka, K.: Acoustic radiation force on fused silica spheres and intensity determination. J. Acoust. Soc. Am. 58, 581-585 (1975)
19. Gorkov, L.: On the forces acting on a small particle in an acoustical field in an ideal fluid. Sov. Phys. Dokl. 6, 773-775 (1962)
20. King, L.: On the acoustic radiation on spheres. Proc. R. Soc. London Ser. A 147, 212-240 (1933)
21. Reynolds, D. D.: Engineering Principles of Acoustics Noise and Vibration Control 1st edn. Allyn and Bacon Inc. (1981)
22. Atkins, P., de Paula, J.: Atkins' Physical Chemistry 7th edn. Oxford University Press (2002)
23. Meriam, J. L., Kraig, L. G.: Engineering Mechanics and Dynamics 4th edn. Wiley (1998)
24. Laurie, H.: MAM3080F, Numerical Methods course notes, Based heavily on "Numerical Analysis", 7th Edition, by Burden and Faires. (2009) Based heavily on "Numerical Analysis", 7th Edition, by Burden and Faires.
25. Doinikov, A.: Acoustic radiation interparticle forces in a compressible fluid. J. Fluid Mech. 444, 1-21 (2001)

APPENDIX A TABLE OF DATA TAKEN TO MEASURE THE DENSITY OF POLYSTYRENE

Table 2 Table of the data taken to measure the density of polystyrene.

	M1a	M1b	M2a	M2b	M3a	M3b	Mean	total wieght (g)	volume (m^3)		Packaging factor		Desnity
Mglass	228.88			228.89		228.9	228.89				0.74		
M700	234.81	238.83	238.68	238.69	238.62	238.62	238.0417	9.151666667	0.0007				17.66731017
Mglass		228.91		228.9		228.91	228.9067						
M500	235.81	235.82	235.9	235.9	235.85	235.85	235.855	6.948333333	0.0005				18.77927928
Mglass		228.91		228.91		228.92	228.9133						
M300	232.87	232.88	233.12	233.13	232.99	233.02	233.0017	4.088333333	0.0003				18.41591592

		total weigl	volume	density
Mwater 700	911	682.1	0.0007	
Mwater 500	707	478.1	0.0005	1020
Mwater 300	511	282.1	0.0003	980
Mwater 200	413	184.1	0.0002	980
Mwater 100	309.77	80.87	0.0001	1032.3
				1003.075

Average Density:	18.28750179

APPENDIX B MECHANICAL DRAWINGS OF A DIFFUSION CHAMBER ACOUSTIC FILTER DESIGN

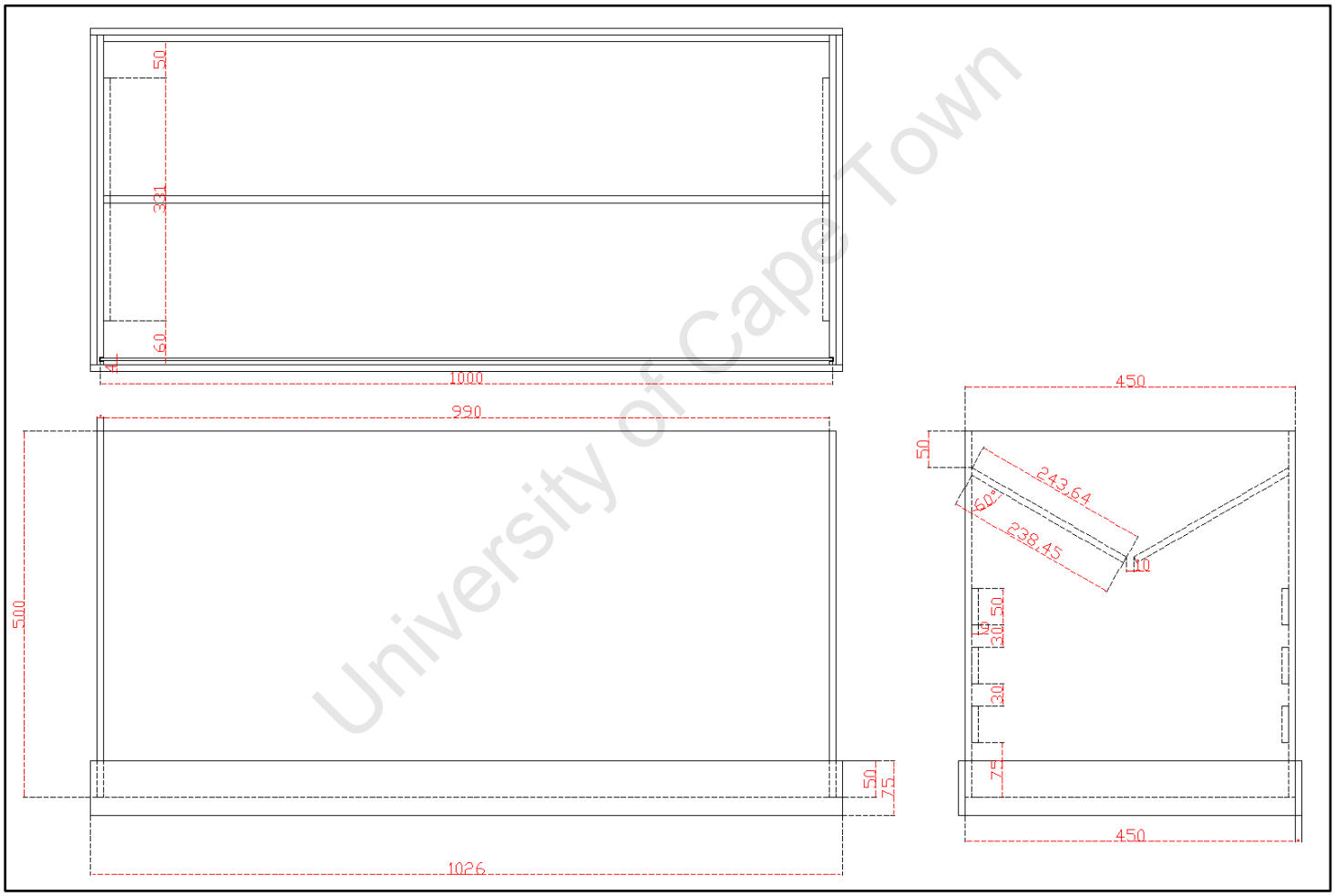

1 Mechanical drawing of the diffuser stage used to spread polystyrene balls evenly over the cross-section of flow. Dimensions in millimetres.

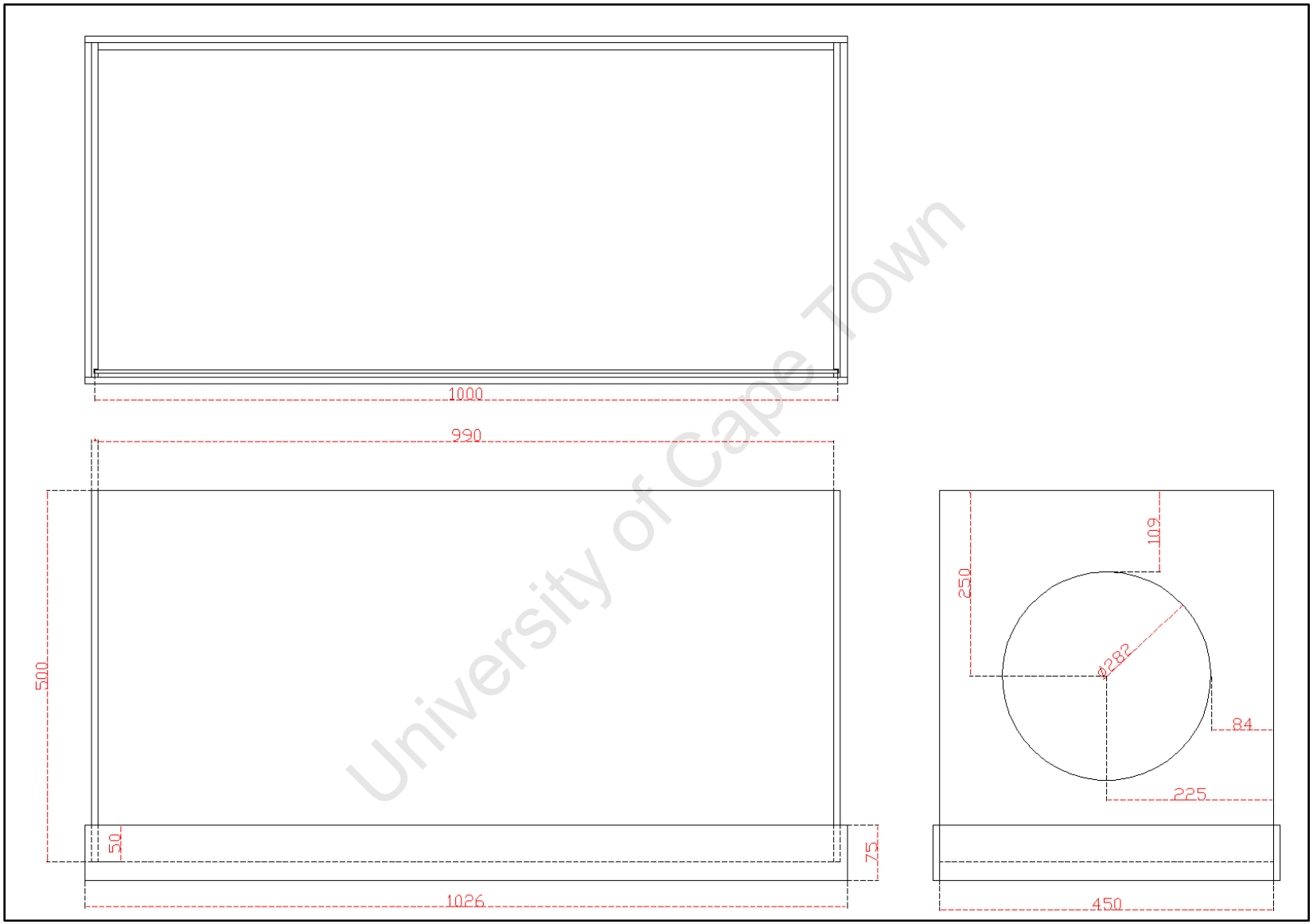

2 Mechanical drawing showing the design of the speaker mounting stage used to apply a pressure standing wave across the longer dimension of the testing rig. Dimensions in millimetres.

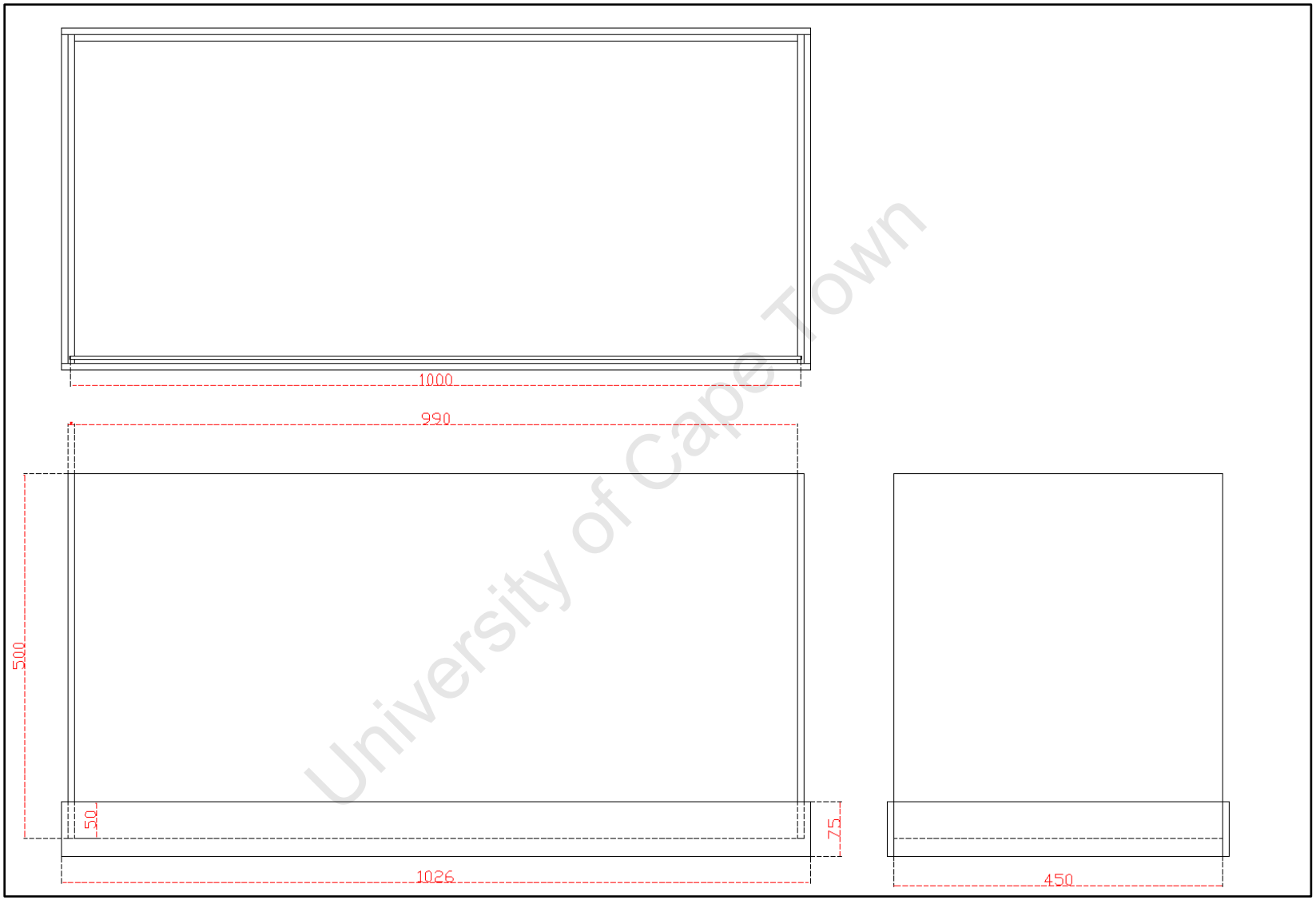

3 Mechanical drawing showing the design of the reflective channel stage used either to allow the polystyrene to reach terminal velocity before entering the sound field or to show how a section of the channel that does not have sound source will resonate with energy that is reflected through the channel. Dimension in millimetres.

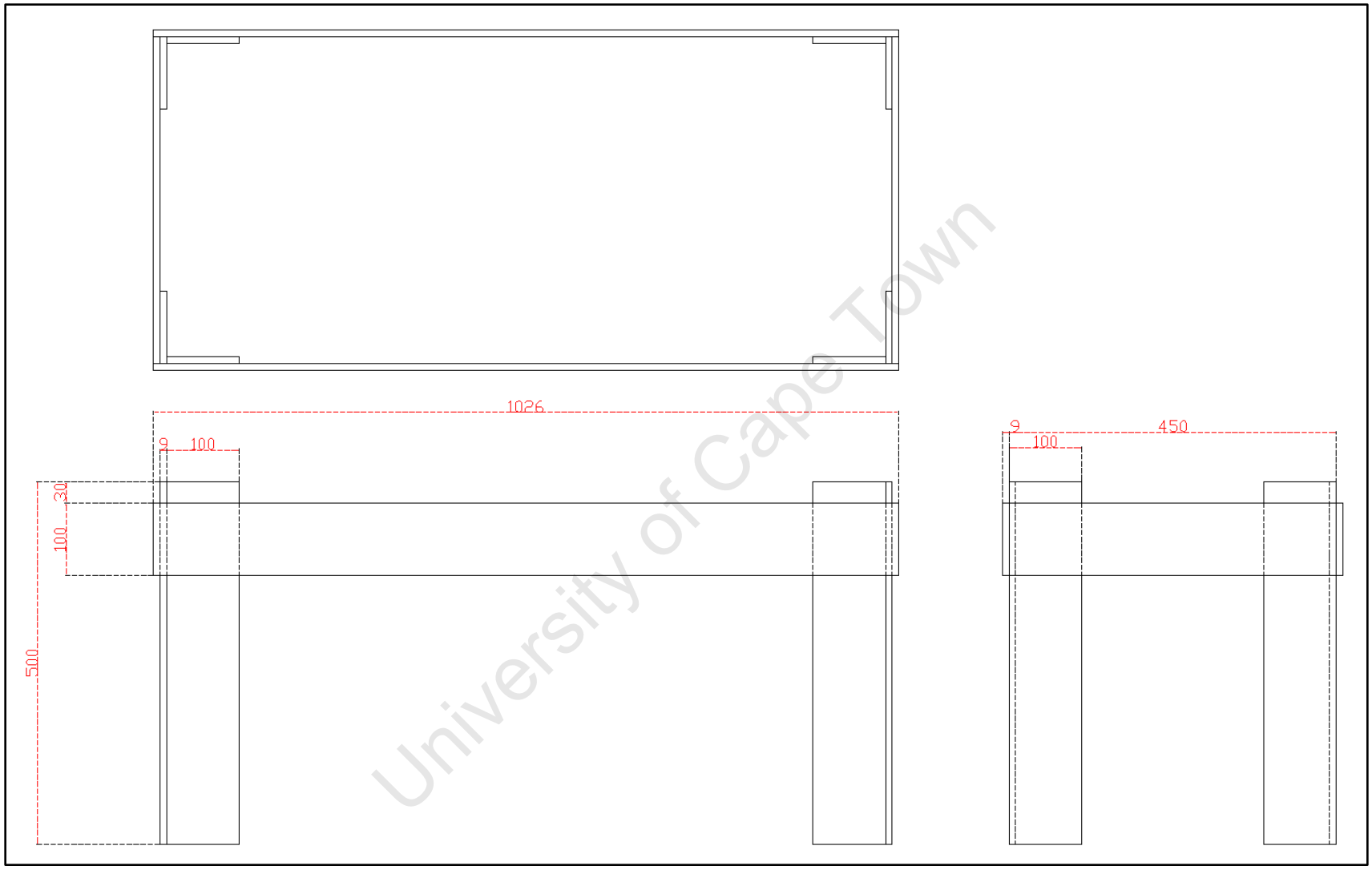

4 Mechanical drawing show the support stage that allows polystyrene balls to be collected from the bottom of the test rig. Dimension in millimetres.

APPENDIX C SUPPLEMENTARY MATERIAL AND DATA

This thesis has been submitted with an accompanying CD containing the following:

C1 – Digital Sources – includes downloaded papers and websites.

C2 – Simulation Code – includes the Matlab code used for the modelling in this thesis

C3 – Mechanical Drawings – includes the mechanical drawings of a diffusion chamber acoustic filter and the design of a cone to focus sound from a speaker into a tube for a Kundt's tube experiment.

C4 – Circuit Schematics – Includes all schematic made during this thesis.